IFN-III is selectively produced by cDC1 and predicts good clinical outcome in breast cancer

Margaux Hubert, Elisa Gobbini, Coline Couillault, Thien-Phong Vu Manh, Anne-Claire Doffin, Justine Berthet, Céline Rodriguez, Vincent Ollion, Janice Kielbassa, Christophe Sajous, et al.

IFN-III is selectively produced by cDC1 and predicts good clinical outcome in breast cancer.

Hubert M, Gobbini E, Couillault C, Manh TV, Doffin AC, Berthet J, Rodriguez C, Ollion V, Kielbassa J, Sajous C, Treilleux I, Tredan O, Dubois B, Dalod M, Bendriss-Vermare N, Caux C, Valladeau-Guilemond J.

Sci Immunol. 2020 Apr 17;5(46):eaav3942.

doi: 10.1126/sciimmunol.aav3942.

Epub 2020 Apr 17. PMID: 32303573.

https://immunology.sciencemag.org/content/5/46/eaav3942

Title:

IFN-III is selectively produced by cDC1 and predicts good clinical outcome in breast cancer

Authors:

Margaux Hubert[1-2], Elisa Gobbini[1,3], Coline Couillault[1], Thien-Phong Vu Manh[4], Anne-Claire Doffin[1], Justine Berthet[1,2], Céline Rodriguez[1,2], Vincent Ollion[1,5], Janice Kielbassa[6], Christophe Sajous[1], Isabelle Treilleux[7], Olivier Tredan[7], Bertrand Dubois[1,2], Marc Dalod[4], Nathalie Bendriss-Vermare[1,2,5], Christophe Caux[1,2,5,7,†], Jenny Valladeau-Guilemond[1,5,†]

Affiliations:

[1] Univ Lyon, Université Claude Bernard Lyon 1, INSERM U1052, CNRS 5286, Centre Léon Bérard, Centre de Recherche en Cancérologie de Lyon, Lyon, 69008, France

[2] Laboratoire d'Immunothérapie des Cancers de Lyon (LICL, Lyon, France)

[3] CHU Grenoble-Alpes, France

[4] Aix Marseille Univ, CNRS, INSERM, Centre d'Immunologie de Marseille-Luminy, Marseille, France

[5] LabEx DEVweCAN, Lyon, France

[6] Synergie Lyon Cancer, Plateforme de Bio-informatique 'Gilles Thomas', Lyon, France

[7] Centre Léon Bérard, F-69008 Lyon, France

[†] These authors contributed equally to this work.

Corresponding author:

Correspondence should be addressed to Jenny Valladeau-Guilemond: Cancer Research Center Lyon, UMR INSERM 1052 CNRS 5286, Centre Léon Bérard, 28 rue Laennec, 69373 LYON cedex 08, FRANCE; Tel : +33 (0)4 78 78 29 64 ; jenny.valladeau@lyon.unicancer.fr;

cDC1-derived IFN-λ is the predominant IFN in breast tumor and its production can be induced through TLR3-mediated cDC1 activation.

Abstract

Dendritic cells play a key role in the orchestration of antitumor immune responses. The cDC1 (conventional dendritic cell 1) subset has been shown to be essential for antitumor responses and response to immunotherapy, but its precise role in humans is largely unexplored. Using a multidisciplinary approach, we demonstrate that human cDC1 play an important role in the antitumor immune response through their capacity to produce type III interferon (IFN-λ). By analyzing a large cohort of breast primary tumors and public transcriptomic data sets, we observed specific production of IFN-λ1 by cDC1. In addition, both IFN-λ1 and its receptor were associated with favorable patient outcomes. We show that IFN-III promotes a Th1 microenvironment through increased production of IL-12p70, IFN-γ and cytotoxic lymphocyte-recruiting chemokines. Finally, we showed that engagement of TLR3 is a therapeutic strategy to induce IFN-III production by tumor-associated cDC1. These data provide insight into potential IFN- or cDC1-targeting antitumor therapies.

Introduction

The use of antitumor immunotherapies such as monoclonal antibodies targeting immune checkpoints (ICPs) has provided promising results for the treatment of several cancers. In spite of favorable outcome of responding patients, the overall response rate remains relatively low, and an ongoing challenge is the identification of new immunotherapy targets. As such, dendritic cells (DCs) represent promising targets owing to their central role in the initiation and the control of immune responses. Their functions encompass a wide range of mechanisms and responses mediated by different subsets namely: the plasmacytoid DCs (pDCs), the two subsets of classical/conventional DCs (cDCs) called CD141/BDCA3^{high} cDC1 and CD1c/BDCA1^{+} cDC2, as well as Langerhans cells (LCs), which display dendritic cell functions although they belong to the macrophage lineage.

The cDC1 population is of particular interest because of their role in the activation of cytotoxic antitumor responses. In mice, these cells were shown to act as professional antigen (Ag) cross-presenting cells to CD8^{+} T cells and are considered to be essential for the induction of antitumor immunity (*1*–*4*) and responses to immunotherapies (*5*–*8*). The superiority of cDC1s relative to other DCs to activate cytotoxic immune responses through Ag cross-presentation has also been shown in humans (*9*–*14*), but their role in antitumor immunity is largely understudied unlike that in mice (*15*). This DC subset was identified in several tumors (*3*, *16*–*18*) and transcriptomic analyses revealed that a high cDC1 infiltration score is associated with favorable patient prognoses (*3*, *4*, *18*–*20*), as well as improved clinical responses to anti-PD-1 therapy in small cohorts of metastatic melanoma patients (*19*). However, the mechanisms underlying the impact of human cDC1 in patient outcomes have not been elucidated.

We previously showed that human cDC1 represent a major source of type III interferon (IFN-III, also called IFN-λ1/2/3 or IL-29/28A/28B) produced in response to TLR3 engagement (*21*, *22*). IFN-III share the same signaling pathway as IFN-I, leading to the transcription of multiple interferon-stimulated genes (ISGs). Similar to IFN-I, IFN-III play a crucial role in autoimmune diseases (*23*) and viral infections (*24*). Their antitumor activity have also been reported in several mouse models (*25*–*28*). In humans, anti-proliferative (*29*, *30*) and pro-apoptotic (*31*, *32*) activities of IFN-III have only been demonstrated *in vitro*. Owing to their specificity of action on a narrow range of cell types, such as epithelial cells and some immune populations, IFN-III-based therapies may potentially lead to fewer toxic side effects compared with IFN-I-based treatments. Thus, investigating the potential production of IFN-III by tumor-associated cDC1 (TA-cDC1) is crucial to unveiling the mechanisms underlying their protective role in antitumor immunity.

Here, we demonstrate that IFN-III is selectively produced by cDC1 in human tumors and is associated with favorable outcomes in breast cancer. Furthermore, we describe the association between cDC1-derived IFN-III and the presence of crucial cytokines and chemokines, including IL-12p70, IFN-γ, CXCR3-L and CX3CR1-L, which promote effector T cell recruitment and activation. Finally, we propose that TLR3 activation of intratumoral cDC1 could be used as a potential therapeutic strategy leading to IFN-III, as well as type 1-related cytokine and chemokine production. These data support the development of therapies targeting cDC1 to trigger IFN-III release resulting in a cytokine microenvironment conducive to the induction of cytotoxic anti-tumor immune responses.

Results

cDC1 are enriched in breast tumors compared with peripheral blood.

To evaluate the infiltration of primary breast tumors by DC populations, we performed multiparametric flow cytometry analysis of freshly dissociated and digested tissues. Among HLA-DR$^+$ lineage$^-$ cells, four discrete TA-DC populations were distinguishable in most tumors (Fig. 1A), namely: pDCs (CD11c$^-$ CD123$^+$), cDC1 (CD11c$^+$ BDCA1$^-$ BDCA3^{hi}), cDC2 (CD11c$^+$ BDCA1$^+$ CD207$^-$) and LCs (CD11c$^+$ BDCA1$^+$ CD207^{hi}). These DC phenotypes were similar to DC subsets previously found in several non-cancerous tissues (*33*) and lung tumors (*17*, *18*). With the exception of LCs that are rarely present in blood, all other DC subsets were detected among peripheral blood mononuclear cells (PBMCs) of patients (fig S1A). We assessed the phenotype of TA-DCs and blood DCs (Fig. 1B, fig S1B) and observed that classical markers such as BDCA2/CLEC4C and CD11b were expressed by pDCs and cDC2, respectively. As in blood, SIRP-α, which is used by CD47-expressing tumor cells to inhibit phagocytosis by APCs (*34*), was expressed by all TA-DCs except cDC1. In contrast, expression of CLEC9A and XCR1 was restricted to TA-cDC1, reinforcing the selection of these two proteins as cDC1-specific markers. Interestingly, cDC1 also expressed the highest level of BTLA, but expressed lower levels of DC-LAMP/CD208 compared with cDC2 and LCs, suggesting a moderate maturation stage (Fig. 1B, fig S2A). Finally, an unsupervised viSNE analysis highlighted the homogeneity of the CLEC9A$^+$ cluster, representing the cDC1 subset in tumor and blood (Fig. 1C, fig S1C), whereas cDC2 and LC populations were more heterogeneous.

Flow cytometry analyses were conducted on a larger cohort of 90 patients harboring all subtypes of breast tumors. As expected, the CD45$^+$ infiltrate varied greatly between tumors (fig S2B). Although cDC1 constitute a discrete population, they were always detectable within CD45$^+$ cells (Fig. 2A-B). Surprisingly, the ratio of cDC1 to all TA-DCs was significantly higher in tumors compared with blood (3.5-fold increase), unlike that of other DC subsets (Fig. 2C), highlighting their likely selective recruitment within tumors and suggesting a potential role of cDC1 in antitumor immunity. By focusing on breast tumor subtypes, we demonstrated a preferential cDC1 infiltration in triple negative breast cancers (TNBCs), which are the most aggressive breast cancers and display the highest level of immune cell infiltration (fig S2C). Indeed, TNBCs also displayed a larger proportion of cDC2 and pDCs compared with other breast cancer subtypes, although this difference was not significant, likely due to a small sample size (fig S2D-E). Conversely, the SBR (Scarff-Bloom and Richardson) grade did not appear to influence the proportion of TA-cDC1, although this may also reflect the small sample size of the SBR1 group (fig S2C-E).

cDC1 are positively correlated with patient survival in many human cancers.

We investigated the prognostic value of cDC1 compared with other DC populations. Based on available transcriptomic data sets of human DCs (*18*, *35–37*), we defined human DC signatures comprised of *CLEC9A* and *XCR1* for cDC1, *CLEC10A* and *CD1E* for cDC2, *CD1A* and *CD207* for LCs, and *CLEC4C* and *LILRA4* for pDCs. The abundance score for each DC population was estimated using gene expression data sets from The Cancer Genome Atlas (TCGA) (*38*) with the MCP-counter algorithm developed by Becht *et al.* (*39*). We assessed the overall survival of patients stratified according to the median of each expression score. This approach revealed the strong association between cDC1 infiltration and a good prognosis in breast cancer (Fig. 3A). Interestingly, cDC2 and LCs, but not pDCs, were also positively correlated with patient survival although to a lesser extent. We extended our analysis to 13 other human cancers and revealed that cDC1 represented the only DC subset associated with a prolonged overall survival in the majority of solid tumors (8/14) (Fig. 3B, fig S3).

Breast tumors highly infiltrated by cDC1 are characterized by an enriched IFN signature.

As cDC1 is the key DC population responsible for effector $CD8^+$ T cell activation, we investigated their precise localization within breast tumors using *CLEC9A* and *CD8A* probes by *situ* hybridization, combined to an opal-based immunofluorescence detection of cytokeratin-positive tumor cells (Fig. 4A). Using the Halo software, 16 zones were randomly defined and quantified for 8 breast tumors. Interestingly, this approach revealed a strong correlation between cDC1 and $CD8^+$ T cells (Fig. 4B). We also observed that cDC1 (*CLEC9A*$^+$ cells) were predominantly localized in the stroma than in the tumor bed (Fig. 4C). Image analysis also highlighted for the first time close contacts between cDC1 and $CD8^+$ T cells in breast tumors (Fig. 4A,C). Indeed, 70% +/- 10% of cDC1 in stroma are in contact with at least one $CD8^+$ T cells (Fig. 4A,C). Using TCGA transcriptomic database of breast cancer, we validated a positive correlation between cDC1 and $CD8^+$ T cell infiltration scores (Fig. 4D). However, this was clearly not a specific feature of cDC1, since this correlation was shared with cDC2 and pDCs. In contrast, LCs and $CD8^+$ T cell infiltration scores were not correlated in tumors, although LCs but not pDCs were associated with a good prognosis (Fig. 3A and Fig. 4D).

In order to gain further insight into the functional specificity of TA-cDC1 associated with their positive prognostic impact, we used the DC infiltration scores defined by MCP-counter to design groups of tumors enriched only in one DC subset. We analyzed their association with gene signature pathways using BubbleGUM (*40*) for high-throughput gene set enrichment analysis (GSEA) of homemade gene sets and of the MSigDB collections. Interestingly, type I/III and type II IFN signatures were strongly enriched in tumors highly infiltrated with cDC1 compared with other groups (Fig. 4E, fig S4A). Hierarchical clustering of type I/III IFN signature genes specifically enriched in cDC1^{high} tumors compared with all other tumor types revealed two groups of genes. The first one (group I) is shared with pDCs^{high} tumors and mostly composed of ISGs, and a second one (group II) containing genes only specific of cDC1 enriched-tumors such as *LPAR6*, *UBA7* or *CSF1* (Fig. 4F). In the type II IFN signature, many genes involved in Ag processing and presentation were highly expressed in cDC1^{high} tumors (*B2M*, *PSMB8*, *HLA-A*, *HLA-B*, *TAPBP*, *PSMB9*, *PSME1*), in addition to genes important for the crosstalk between NK cells and DCs such as *HLA-A* and *–B*, *IL-15R* and *IL-15*. Interestingly, *CD274*/*PD-L1* was particularly enriched in cDC1^{high} tumors (Fig. 4F). Although no pathway was specifically enriched in cDC2^{high} tumors, these tumors seem to have the lowest IFN signatures (Fig. 4E). The signatures related to G2M checkpoint and hypoxia were enriched in LC^{high} tumors compared with other groups (Fig. 4E). On the other hand, while the TNF-α signaling pathway was predominantly associated with cDC1, cDC2 or LCs compared with pDCs, oxidative phosphorylation and immunosuppressive pathways were distinctive of pDC^{high} tumors (Fig. 4E). This last result is in line with the correlation between pDCs and regulatory T cells (Tregs) in breast tumors compared with other DC subsets (r = 0.6042) (fig S4B), and corroborates our previous observations (*41*). Finally, in comparison with cDC1^{high} tumors, tumors highly infiltrated by pDCs, LCs or cDC2 presented with a more mesenchymal phenotype, as evidenced by the enriched EMT signature (Fig. 4E and fig S4A). This *in silico* analysis revealed an association between cDC1 and the presence of a strong IFN signature in human breast tumors.

IFN-λ1 is selectively produced by cDC1 in breast tumors.

IFN-III production is a well-known feature of cDC1 (*21*, *22*) that has been characterized during viral infections, but neither the presence of this cytokine nor its role have been investigated in human tumors. The enrichment in the type I/III IFN signature in cDC1-exclusive tumors prompted us to analyze the link between IFN-III and TA-cDC1. We initially demonstrated the upregulation of IFNL1 gene expression in tumoral compared with normal adjacent tissue (NAT), based on TCGA transcriptomic data sets of multiple cancers (Fig. 5A), confirming the presence of IFN-III in tumors. Interestingly, this differential expression

between tumor and NAT was highly significant for breast, head and neck and lung cancers in which cDC1 are strongly associated with favorable patient outcome (Fig. 3B). We confirmed the presence of IFN-λ1 at the protein level in 87/106 soluble tumor milieu (STMs) samples obtained by mechanical dissociation of breast tumors, with a concentration ranging from 10 to 800 pg/mL in half of the tumors (Fig. 5B). Of note, IFN-λ2 was also detected in these STMs and highly correlated with IFN-λ1 (fig S5A). In addition, IFN-λ1 was the most abundant IFN subtype in breast tumors compared with type I IFNs (fig S5B). Indeed, IFN-α was completely absent and IFN-β was detected at a very low concentration (< 50 pg/mL) in only 30% of STMs (fig S5B), consistent with our previous demonstration of the inability of TA-pDCs to produce IFN-α in breast tumors (*41*). These results are in complete agreement with mRNA levels of all IFN subtypes in the TCGA breast cancer data set, showing high expression of genes coding for IFN-III, whereas all of the *IFNA* genes were below the detection threshold (fig S5C). Intracytoplasmic flow cytometry analysis revealed spontaneous production of IFN-λ1 that is restricted to cDC1 in the absence of any *ex vivo* stimulation in a third of the tumors (4/12) (Fig. 5C-D). Of note, we also detected TNF-α production, mostly by TA-cDC2, but no IFN-α (fig S5D). To confirm these findings, double fluorescent RNA *in situ* hybridization was performed with *IFNL1* and *CLEC9A* probes (Fig. 5E). Using Halo software, 16 zones of 0.64 mm^2 were randomly defined and quantified for 6 breast tumors (representing a total area per tumor of ~12 mm^2). This approach confirmed the presence of *IFNL1* transcripts in *CLEC9A*$^+$ TA-cDC1 in 2/6 tumors (Fig. 5E-G). Of note, tumors in which IFN-λ1 was detected appeared to be more infiltrated by cDC1 (fig S5E). In addition, *IFNL1* was absent from cytokeratin-positive tumor cells (Fig. 5E). These results clearly indicate that IFN-λ1 production is a specific feature of cDC1 in a human tumor context and that this cytokine may play a central role in their antitumor activity.

IFN-λ1 is associated with a better survival and induces a Th1 soluble microenvironment in human breast tumors.

We explored the prognostic impact of *IFNL1* and of *IFNLR1,* the specific chain of its heterodimeric receptor, using public transcriptomic data sets. High expression level of these two genes correlated with greater relapse-free survival (RFS) (Fig. 6A). To understand the mechanisms underlying the beneficial impact of type III IFN on cancer, we dissected the soluble tumor microenvironment by quantifying multiple cytokines and chemokines in the STM of more than 100 dissociated breast tumors. Interestingly, IFN-λ1 was strongly correlated with CXCR3-L (CXCL11 / CXCL10 / CXCL9) and CX3CL1 chemokines, as well as TNF-α and IL-12p40 (Fig. 6B, fig S6). These results raised the hypothesis that the production of IFN-λ1 by cDC1

in tumors could be associated with cytokines and chemokines involved in the recruitment and activation of cytotoxic lymphocytes (NK cells and $CD8^+$ T cells). To test this hypothesis, we assessed the impact of IFN-λ1 on the tumor microenvironment by treating human breast tumor suspensions with IFN-λ1 for 24h. We showed that IFN-λ1 is a potent inducer of IFN-β but does not induce IFN-α2 (Fig. 6C). In addition, the level of cytotoxic lymphocyte-attracting chemokines was largely increased, in particular for two CXCR3-L (CXCL10 and CXCL11) and for CX3CL1 (Fig. 6C). Importantly, IFN-λ1 activation alone induced IL-12p70 production, a key cytokine for the differentiation and activation of Th1 lymphocytes and of effector $CD8^+$ T cells, as well as high amounts of IFN-γ (Fig. 6C). Together these results demonstrate a role for type III IFNs in the induction of a Th1 immune soluble microenvironment in human breast tumors.

TLR3 stimulation is a potent strategy to induce the production of IFN-λ1 by cDC1 and Th1-related immune responses in breast tumors.

Given the positive prognostic impact of IFN-λ1 in breast cancer and its putative role in the recruitment and activation of cytotoxic immune cells, we speculated that the induction of IFN-III could be a potential therapeutic strategy in combination with other immunotherapies. Several studies reported the involvement of TLR3 signaling in the activation of IFN-λ production by cDC1 (*21*, *22*). Thus, we treated patient PBMCs or breast tumor cell suspensions with polyinosinic-polycytidylic acid (poly(I:C), double stranded RNA), a TLR3 agonist to target cDC1, in addition to resiquimod (R848, single stranded RNA) to stimulate other DC subsets through TLR7/8. As expected, this combined activation led to TNF-α production by all patient blood DC subsets (fig S7), IFN-α by pDCs, as well as IFN-λ1 both by cDC1 and by pDCs (Fig. 7A-B). In tumor cell suspensions, we confirmed the impairment of TA-pDC to produce IFN-α and demonstrated their inability to produce IFN-λ1 as well (Fig. 7A-B), in contrast to patient blood pDCs. Interestingly, unlike TA-pDCs, TA-cDC1 were responsive to TLR stimulation and could efficiently produce IFN-λ1 in 11 out of 12 tumors (Fig. 7A-B). This activation also led to TNF-α production by all TA-DCs (fig S7). We also evaluated the global impact of such TLR3 stimulation on the tumor microenvironment. Multiple cytokines and chemokines were quantified in the supernatant of *ex vivo* PolyI:C-stimulated fresh breast tumor thick sections instead of tumor cell suspensions in order to conserve the tissue architecture. We observed a strong induction of IFN-λ1 upon TLR3 triggering (Fig. 7C). The production of IFN-γ, CXCL9, CXCL10 and CX3CL1 was significantly increased (Fig. 7C), thus highlighting the potential of cDC1 stimulation in tumor tissue *via* TLR3-L to induce a microenvironment favorable to recruitment and activation of cytotoxic effector cells.

Discussion

Our study highlights a crucial function of human cDC1 in anti-tumor immunity through their capacity to specifically produce type III IFN. Indeed, while little or no type I IFN is present in human breast tumors, IFN-III is produced in over 50% of patients. Here, we uncover a key role for IFN-III in the induction of IL-12p70, IFN-γ, CXCR3-L and CX3CL1, cytokines and chemokines involved in the recruitment and activation of NK and effector T cells, and reveal that the expression of *IFNL1* or *IFNLR1* genes is associated with a favorable patient outcome.

We demonstrated that cDC1 are the source of IFN-III in the breast tumor environment. This was observed by flow cytometry showing that among immune and non-immune cells only cDC1 spontaneously expressed IFN-λ1 in 1/3 of tumors, and to a less extent, in patient blood. This was validated by *in situ* hybridization, demonstrating that IFN-λ1 was only expressed by cDC1 in primary breast tumors. In accordance with the specific expression of IFN-λ in cDC1, our *in silico* analysis showed that the type I/III gene signature was enriched in tumors highly infiltrated with cDC1 compared with other DC types. Whereas IFN-III expression was reported in epithelial cells, hepatocytes, monocyte-derived DCs, pDCs and cDCs in response to many viral infections such as hepatitis B and C viruses, herpes simplex virus (*42*–*44*) and non-viral nucleic acids (*45*), we and others have shown that cDC1 produce large amounts of IFN-III upon TLR3 stimulation (*21*, *22*). The spontaneous production of IFN-III specifically by cDC1 tumors suggest that they are activated in the breast tumor environment, possibly through TLR3 ligands such as double-stranded RNA, including endogenous retroviruses (*46*). Other intracellular sensors such as Ku70 are involved in IFN-III production in response to exogenous DNA through STING activation, and may also be implicated in tumors (*47*).

By analyzing a number of cytokines and chemokines secreted in a large cohort of breast cancer patients, we highlighted the strong correlation between IFN-λ1 and CXCL9/10/11, the three ligands of CXCR3, a chemokine receptor strongly expressed by Th1, CTL, NK and NKT cells (*48*). In this context, molecules increasing paracrine expression of these CXCR3-L have been shown to initiate antitumor immunity in many models (*49*). We observed that IFN-λ1 is also correlated in the TME with CX3CL1, a chemokine involved in the recruitment of effector T cells endowed with particularly high cytotoxic activity (*50*). These last results raise the hypothesis of IFN-III involvement in cytotoxic immune cell recruitment in the tumor. By inducing the same core of genes as IFN-I (*51*), IFN-III may play a key role in the antitumor immune response. IFN-I is already known to be an inducer of cDC maturation (*52*), and it appears to

strongly enhances cross-presentation, which is critical for the induction of $CD8^+$ T cell responses against cancer (*53*). Here, we show that treatment of tumor cell suspensions with recombinant IFN-λ1 induces production of IFN-β and IFN-γ, revealing an amplification loop between these different IFN subtypes. The capacity of IFN-III to induce IFN-γ and IL-12p70 suggests a direct or indirect effect on T or NK effector cells, leading to their activation. In mice, it was shown that IFN-III acts directly on NK cells (*26*, *27*, *54*) but the effects of IFN-λR1 on human NK or T cells has not been reported, suggesting a more indirect effect in human tumors. In line with these observations, we demonstrated through *in silico* analyses that cDC1-enriched tumors are associated with a type II IFN signature. Thus, these data suggest that the endogenous activation of cDC1 will not only favor cytotoxic effector recruitment through CXCR3-L or CX3CL1, but will also induce their activation. We have previously demonstrated that IL-12p70 production induced by TLR activation of human DCs was dependent on autocrine type I IFN (*55*). Thus, a loop of IFN-III signaling may be necessary in tumors for bioactive IL-12p70 secretion by conventional DCs. Finally, even though IFN-I and IFN-III activate the same signaling pathway, they clearly induce different responses in tumors, likely through different expression patterns of their receptors. Indeed, in humans, few papers reported the expression of IFN-λR1 in epithelial cells of the airways and intestinal tract, and in blood on B cells and pDCs (*56*). Indeed, human pDCs respond to IFN-III (*57–59*) through the canonical JAK-STAT pathway (*60*, *61*), leading to the upregulation of ISG expression (*60–62*) and type I IFN production (*61*). The cross-talk between pDCs and cDC1 through type I/III IFNs for anti-tumor immunity has previously been established in mouse tumor models (*63*). Human B cells also respond to IFN-III by upregulating ISGs (*44*, *56*, *60*). In addition, it was reported that epithelial cell polarization and differentiation can influence the expression of IFN-λR1 in mice (*64*), and that histone deacetylase inhibitors confer IFN-III responsiveness to previously non-responsive human cell lines (*65*). These findings suggest that the variable expression of the *IFNLR1* gene in the tumor microenvironment could also modulate its responsiveness to IFN-III. Therefore, it will be important to precisely identify the intra-tumoral cell population directly responding to IFN-III.

We have also shown that cDC1 clearly display the highest positive prognostic impact in breast cancer compared with other DC subsets. This observation extends results from two studies suggesting the association between breast tumor infiltration by cDC1 and a favorable prognosis (*3*, *4*). We demonstrated that the cDC1 signature has a positive prognostic impact in several other tumor types (8 out of 14), in particular in lung, head and neck, and metastatic melanoma, all responding to T cell immune checkpoint therapies. Interestingly, no prognostic impact was found in aggressive cancers, such as ovarian or pancreatic tumors, which have been found to be less sensitive to immunotherapy thus far. With respect

to other DC subsets, a high infiltration of breast tumors by cDC2 and LCs is associated with an increased overall survival, although this association is of a lower significance compared with cDC1. In contrast with their association with a favorable outcome of breast cancer patients, LCs are not correlated with $CD8^+$ T cells but are associated with a hypoxic gene signature in breast tumors. This may be due to their presence within the tumor islets (*66*), in contrast to all other DC subsets preferentially localized in T cell aggregates. Unlike cDCs and LCs, the pDC signature has no impact on breast patient outcome. Furthermore, in GSEA analyses, immunosuppression and oxidative phosphorylation (OXPHOS) pathways were higher in pDC^{high} tumors, which corroborates our previous demonstration of the role of pDCs in breast cancer progression by promoting Tregs accumulation (*67*), and with another study supporting the implication of OXPHOS in the survival of Tregs (*68*). We also observed the EMT signature enrichment in cDC2/LC/pDC^{high} compared with $cDC1^{high}$ tumors, which is relevant with data highlighting the EMT as an immune evasion mechanism contributing to metastatic dissemination (*69*). Nevertheless, all those *in silico* analyses of patient survival have to be validated by *in situ* staining on large cohorts. In this context, the *in situ* identification of cDC1 was hampered by the lack of specific mAb against CLEC9A or XCR1. Here, we visualized $CLEC9A^+$ cDC1 in human tumors by *in situ* fluorescent hybridization. cDC1 have been characterized in NSCLC, colorectal cancer and melanoma using the staining of IRF8 or CD141/BDCA3 staining (*16*, *17*), two markers also respectively expressed by pDCs and cDC2. Thus, we believe that CLEC9A is a better cDC1 marker based on our extended flow cytometry analysis and by the recent characterization of Zilionis *et al.* who performed single-cell RNA sequencing of lung tumors and demonstrated that TA-cDC1 have a high level of *CLEC9A* and *XCR1* mRNA (*18*). We also observed that cDC1 are localized in lymphoid aggregates *in situ*, where they establish direct interactions with $CD8^+$ T cells. This is in accordance with the correlation we observed by *in silico* analysis between cDC1 and $CD8^+$ T cell scores, which was also previously reported in multiple solid tumors (*4*) including metastatic melanoma (*6*). However, we reported here that the strength of this association is comparable to the other DC subsets, and thus could not explain by itself the better prognostic impact of cDC1, strengthening the importance and specificity of type III IFN production by cDC1.

Finally, in contrast to TA-pDC impairment for their IFN-λ1 production in response to TLR7/8 ligand, as we previously showed for IFN-α (*41*, *70*), we now highlight the potency of a TLR3 agonist to induce IFN-λ1 production by TA-cDC1. We demonstrated the induction of CX3CL1 and CXCL9/10 production through tumor cell suspensions stimulation with a TLR3 agonist. These chemokines could be produced by cDC1 themselves, as previously demonstrated in blood (*22*). Their activation in tumors may directly lead to the secretion of both IFN and cytotoxic lymphocyte-recruiting chemokines, thus creating a favorable

environment to boost antitumor immunity. TLR3 triggering presents promising results for the development of new combined therapies, including with ICP blockers. In melanoma-engrafted mice, the intra-tumoral administration of PolyI:C, combined to the cDC growth factor FLT3-L, significantly enhances the immunotherapeutic response of ICP inhibiting treatments. Furthermore, the beneficial effect of this treatment was demonstrated to be IFN-I-dependent (*7*). As IFN-I and -III share the same signalization pathway, and as suggested by our results, the induction of IFN-III production by TLR3-L might be involved in this process as well. Finally, the treatment of tumors by PolyI:C could also be beneficial to activate the MDA5/RIG-I pathway, which is known to directly induce the production of IFN-I by non-hematopoietic cells and to directly act on tumor cells (*71*). Due to the small size of fresh human breast tumors, it seems for now infeasible to perform functional analyses of IFN-III producing cDC1, for example to investigate their Ag cross-presentation ability. Thus, the particular role of those activated cDC1 would have to be further explore in animal studies. Furthermore, the kinetics of this IFN-III production during the early stage of immune surveillance would be very important to analyze, using for example IFN-III GFP reporter mice. Finally, further studies will be necessary to test whether our observation extends to others solid tumors.

Overall, these data suggest that cDC1 have a positive impact on patient survival, likely involving type III IFN production. This synthesis may be initiated by TLR3-mediated detection of endogenous double-stranded RNA (*46*) released during tumor remodeling. The endogenous signal leading to the IFN-III production by TA-cDC1 remains to be identified. However, our demonstration of potential anti-tumor functions of IFN-III provides valuable evidence to support the development of new therapeutic strategies targeting cDC1 to amplify the response to immunotherapies, especially in breast cancer.

Materials and Methods

Study design. The objective of this study was to investigate the role of cDC1 and their IFN-III production in the anti-tumor immune responses. To this end, freshly resected breast tumors were dissociated into cell suspensions or cut into thick sections before performing flow cytometry and electrochemiluminescence assays. We also used FFPE tumor samples for *in situ* hybridization and immunofluorescence assays. Finally, we analyzed publicly available transcriptomic data sets of various solid tumors. The sample size per group, the experimental replicates, as well as the statistical methods, are described in each figure legend.

Study approval. All human samples (blood and tumors) were obtained after approval from the Institutional review board and ethics committee of the CLB (L-06-36 and L-11-26) and patient written informed consent, in accordance with the Declaration of Helsinki.

Breast cancer patients. We enrolled patients diagnosed with primary breast carcinoma. Fresh tumors and blood samples (collected in EDTA anticoagulant-containing tubes) were obtained from the Biological Resources Center (BRC) of the Centre Léon Bérard (CLB, BB-0033-00050, Lyon, France) and from the TUMOROTHEQUE (BRC of the Hospices Civils de Lyon, France). Tumors were used for single cell suspensions preparation, *ex vivo* culture of thick section or formalin-fixed paraffin-embedded (FFPE) for *in situ* stainings. Healthy human blood (collected in EDTA anticoagulant-containing tubes) was purchased anonymously from the Etablissement Français du Sang (EFS, Lyon, France).

PBMC isolation and tumor cell suspensions. Sections of the resected tumor were selected by the pathologists. 500 µg of fresh tissues was mechanically dissociated in 1mL of RPMI 1640 medium (Gibco) with antibiotics (100 IU/mL penicillin and 100 µg/mL streptomycin, Invitrogen). The supernatant of dissociated tumors, referred thereafter as soluble tumor milieu (STMs), was immediately collected and stored at -80°C for subsequent cytokine and chemokine quantification. Tissues were then digested for 45 min at 37°C in RPMI 1640 with antibiotics, 1 mg/mL of collagenase IA and 20 µg/mL of DNase I (Sigma Aldrich). Digested samples were then filtered on a 70 µm cell strainer and re-suspended in RPMI 1640 with antibiotics and supplemented with 10% FCS (complete RPMI) for further analysis.

Peripheral blood mononuclear cells (PBMCs) were isolated from blood samples of patients or healthy donors through Ficoll density gradient centrifugation (Eurobio).

***Ex vivo* stimulation.** Tumor cell suspensions and PBMC were cultured at $1x10^6$ cells/mL for 5 h in complete RPMI with different activators: 5 µg/mL R848 (Invivogen) and 30 µg/mL PolyI:C (Invivogen). GolgiPlug (BD Biosciences) was added after 1 h. At the end of the activation, harvested cells were stained for membrane markers, fixed, permeabilized and stained for intracellular cytokines. Tumor cell suspensions were also activated for 48 h with 100 ng/mL IFN-λ1 (R&D) for cytokine quantification by ECLIA, which is the most sensitive assay for protein quantification.

To preserve subcellular architecture, 200 µm sections of fresh tumors were cut using a vibratome. These sections were incubated for 48 h with 100 µg/mL PolyI:C (Invivogen) and supernatants were collected for cytokine quantification by ECLIA.

Cell staining and flow cytometry. Single cell suspensions were stained using antibodies listed in Table S1. Dying cells were excluded by Zombie Violet/Yellow staining (Biolegend) depending on the experiment. Lymphocytes, NK cells, neutrophils and other myeloid cells (monocytes, macrophages and inflammatory monocytes) were also excluded using respectively anti-CD3/56/15/14 antibodies in the lineage. Intracellular cytokine or DC-LAMP staining were performed after fixation and permeabilization (Fix/Perm buffers, eBioscience). All flow cytometry acquisitions were done on a LSRFortessa Cell Analyzer (BD Biosciences) and data were processed in FlowJo 10.4 (Tristar). Some flow cytometry data were visualized using viSNE (Cytobank) (*72*), a dimensionality reduction method which uses the Barnes-Hut acceleration of the t-SNE algorithm. viSNE plots were generated separately for each patient.

Cytokine and chemokine quantification by MSD assay. The following cytokines and chemokines were quantified in STMs or in supernatants of activated thick tumor sections and tumor cell suspensions, using ECLIA (electrochemiluminescence assay) and MSD technology according to the U-plex protocol (MSD): IL-1α, IL-1β, IL-6, IL-8, IL-12/IL-23p40, IL-12p70, IL-17A, IL-18, IL-23p19, IL-33, IFN-α2a, IFN-β, IFN-γ, IFN-λ, CX3CL1, TNF-α, CXCL9, CXCL10, CXCL11, TGF-β1, TGF-β2, TGF-β3.

***In situ* hybridization (ISH) combined with immunofluorescence on FFPE tumor sections.** FFPE tumors were cut into 4 µm sections. *In situ* probe hybridization combined with immunofluorescence was performed on the Leica BOND RX System. This procedure is based on the standard RNAscope LS Multiplex Fluorescent Assay. Tumor slides were rehydrated and deparaffinized before fixation, protease pretreatment, probe hybridization (Hs-*CLEC9A*-C2 probe in combination with Hs-*CD8A*-C1 or Hs-*IFNL1*-C1 probes), amplification and anti-cytokeratin staining. Opal dyes (Perkin Elmer) were used for fluorescent detection of probes and anti-cytokeratin antibody. Nuclei were then counterstained with DAPI and slides were scanned using the Vectra Polaris automated quantitative pathology imaging system (Perkin Elmer). Finally, the Halo software (Indica Labs) was used to randomly defined 16 zones of per tumor (0.64 mm^2/zone, 11.88 mm^2 total for *CLEC9A*/*IFNL1*; 0.99 mm^2/zone, 15.84 mm^2 total for *CLEC9A*/*CD8A*), and to quantify positive cells. Contacts between each cDC1 and at least one $CD8^+$ T cells were manually quantified.

Survival analysis. The clinical outcome data and RSEM normalized expression datasets from The Cancer Genome Atlas (TCGA) were downloaded from the cBioPortal (provisional data, February 2018) for 14 tumor types: bladder carcinoma (BLCA), breast invasive carcinoma (BRCA), colorectal adenocarcinoma (COAD), brain lower grade glioma (LGG), head and neck squamous cell carcinoma (HNSC), kidney renal papillary cell carcinoma (KIRP), liver hepatocellular carcinoma (LIHC), lung adenocarcinoma (LUAD), ovarian serous cystadenocarcinoma (OV), pancreatic adenocarcinoma (PAAD), prostate adenocarcinoma (PRAD), skin cutaneous metastatic melanoma (SKCM), stomach adenocarcinoma (STAD) and thyroid cancer (THCA). MCPcounter (*39*) was used to estimate the relative abundance of several population of immune cells. This algorithm originally allows the quantification of the absolute abundance of eight immune populations and two stromal cell populations in heterogeneous tissues from transcriptomic data. Here, in addition to the original cell population signatures defined by Becht *et al*, the following gene signatures were used to run MCPcounter: cDC1 (*CLEC9A, XCR1*), cDC2 (*CLEC10A, CD1E*), pDCs (*LILRA4, CLEC4C*) and LC (*CD207, CD1A*). Overall survival analyses and plots were performed with R, using the packages *survival* and *survminer*. For each immune population, we compared patients displaying the top 50% highest level of infiltration by the given immune cell type and those with the 50 % lowest level. The log-rank test was used to determine statistical significance for overall survival between this two groups of patients. Analysis of progression-free survival was performed for the top 50% and bottom 50% *of IFNL1* and *IFNLR1* gene expression ranked values using the Kaplan Meier plotter software (*73*).

Gene expression analysis. RNAseq data for 14 types of solid human cancers and matched normal samples were downloaded using the *TCGABiolinks R*-package (open access data from the TCGA data portal, version March 2018) with the harmonized option (data aligned to hg38). For each cancer type, HT-Seq raw read counts were normalized using the *DESeq2 R*-package and log2 transformed. Wilcoxon tests were performed to assess whether the *IFNL1* gene was differentially expressed between tumor and normal samples.

Heatmaps and hierarchical clustering. Heatmaps of Log2-normalized expression values of selected genes were performed using the Morpheus website from the Broad Institute (https://software.broadinstitute.org/morpheus/). Hierarchical clustering was performed using the One-Pearson correlation as a metric and the complete linkage as a clustering method for genes.

Gene set enrichment analysis. In order to gain insight into the functional specificity of TA-DC subsets, we used the DC infiltration scores defined by MCP-counter to design groups (n = 48 for cDC1, n = 18 for cDC2, n = 95 for LCs and n = 67 for pDCs) with a high infiltration score for one DC subset (score > median of all tumors) and low for the 3 other subsets (score < median of all tumors). Using these groups, high-throughput gene set enrichment analyses were performed using the BubbleMap module of BubbleGUM (*40*). BubbleMap analysis was performed with 1,000 gene set-based permutations, and with "Signal2noise" as a metric for ranking the genes. The results are displayed as a bubble map, where each bubble is a GSEA result and summarizes the information from the corresponding enrichment plot. The color of the Bubble corresponds to the tumors from the pairwise comparison in which the gene set is enriched. The bubble area is proportional to the GSEA normalized enrichment score. The intensity of the color corresponds to the statistical significance of the enrichment, derived by computing the multiple testing-adjusted permutation-based P value using the Benjamini–Yekutieli correction. Enrichments with a statistical significance above 0.25 are represented by empty circles. Public gene sets of the Hallmark collection (v6.1) were downloaded from MSigDB (*74*) and homemade gene sets are detailed in Table S2. Of note, as IFN-III share the same signaling pathway and induce similar ISGs than IFN-I, we renamed the type I IFN Hallmark signature into type I/III IFN signature.

Statistics. Wilcoxon or paired t tests for paired samples, and Mann-Whitney tests for unpaired samples, were performed for the comparison of two groups. To compare more groups, Kruskall-Wallis tests were performed for unpaired samples and Friedman tests for paired samples. All graphs show each sample value. The horizontal bars represent the median for each group of samples. The bar plot represents the mean with the SEM for each group of samples. Statistical significance: *p<0.05, **p<0.01, ***p<0.001, ***p<0.0001

Supplementary materials:

- **Fig. S1.** Identification of DC subsets in patient PBMCs.
- **Fig. S2.** Proportion of DCs among the immune infiltrate of breast
- **Fig. S3.** Kaplan-Meier analysis of the overall survival of cancer patients (Part 1 and 2).
- **Fig. S4.** *In silico* analysis of pathways associated to each DC infiltration score.
- **Fig. S5.** Quantification of IFNs in breast tumors.
- **Fig. S6.** Correlations between the soluble factors present in human tumors.
- **Fig. S7.** Analysis of the TNF-α production by DC subsets infiltrating breast tumors.
- **Table S1.** FACS antibodies
- **Table S2.** Immunosuppression gene signature

References:

1. K. Hildner, B. T. Edelson, W. E. Purtha, M. Diamond, H. Matsushita, M. Kohyama, B. Calderon, B. U. Schraml, E. R. Unanue, M. S. Diamond, R. D. Schreiber, T. L. Murphy, K. M. Murphy, Batf3 Deficiency Reveals a Critical Role for CD8α+ Dendritic Cells in Cytotoxic T Cell Immunity. *Science*. **322**, 1097–100 (2008).

2. M. B. Fuertes, S.-R. Woo, B. Burnett, Y.-X. Fu, T. F. Gajewski, Type I interferon response and innate immune sensing of cancer. *Trends in Immunology*. **34**, 67–73 (2013).

3. M. L. Broz, M. Binnewies, B. Boldajipour, A. E. Nelson, J. L. Pollack, D. J. Erle, A. Barczak, M. D. Rosenblum, A. Daud, D. L. Barber, S. Amigorena, L. J. van't Veer, A. I. Sperling, D. M. Wolf, M. F. Krummel, Dissecting the Tumor Myeloid Compartment Reveals Rare Activating Antigen-Presenting Cells Critical for T Cell Immunity. *Cancer Cell*. **26**, 638–652 (2014).

4. J. P. Böttcher, E. Bonavita, P. Chakravarty, H. Blees, M. Cabeza-Cabrerizo, S. Sammicheli, N. C. Rogers, E. Sahai, S. Zelenay, C. R. E. Sousa, NK Cells Stimulate Recruitment of cDC1 into the Tumor Microenvironment Promoting Cancer Immune Control. *Cell*. **172**, 1022–1037.e14 (2018).

5. S. Spranger, R. Bao, T. F. Gajewski, Melanoma-intrinsic β-catenin signalling prevents anti-tumour immunity. *Nature*. **523**, 231–5 (2015).

6. S. Spranger, D. Dai, B. Horton, T. F. Gajewski, Tumor-Residing Batf3 Dendritic Cells Are Required for Effector T Cell Trafficking and Adoptive T Cell Therapy. *Cancer cell*. **31**, 711–723.e4 (2017).

7. H. Salmon, J. Idoyaga, A. Rahman, M. Leboeuf, R. Remark, S. Jordan, M. Casanova-Acebes, M. Khudoynazarova, J. Agudo, N. Tung, S. Chakarov, C. Rivera, B. Hogstad, M. Bosenberg, D. Hashimoto, S. Gnjatic, N. Bhardwaj, A. K. Palucka, B. D. Brown, J. Brody, F. Ginhoux, M. Merad, Expansion and Activation of CD103(+) Dendritic Cell Progenitors at the Tumor Site Enhances Tumor Responses to Therapeutic PD-L1 and BRAF Inhibition. *Immunity*. **44**, 924–38 (2016).

8. A. R. Sánchez-Paulete, F. J. Cueto, M. Martínez-López, S. Labiano, A. Morales-Kastresana, M. E. E. Rodríguez-Ruiz, M. Jure-Kunkel, A. Azpilikueta, M. A. Aznar, J. I. I. Quetglas, D. Sancho, I. Melero, Cancer Immunotherapy with Immunomodulatory Anti-CD137 and Anti-PD-1 Monoclonal Antibodies Requires BATF3-Dependent Dendritic Cells. *Cancer discovery*. **6**, 71–9 (2016).

9. A. Bachem, S. Güttler, E. Hartung, F. Ebstein, M. Schaefer, A. Tannert, A. Salama, K. Movassaghi, C. Opitz, H. W. Mages, V. Henn, P.-M. M. Kloetzel, S. Gurka, R. A. Kroczek, Superior antigen cross-presentation and XCR1 expression define human CD11c+CD141+ cells as homologues of mouse CD8+ dendritic cells. *The Journal of experimental medicine*. **207**, 1273–81 (2010).

10. K. Crozat, R. Guiton, V. Contreras, V. Feuillet, C.-A. A. Dutertre, E. Ventre, T.-P. P. V. Manh, T. Baranek, A. K. Storset, J. Marvel, P. Boudinot, A. Hosmalin, I. Schwartz-Cornil, M. Dalod, The XC chemokine receptor 1 is a conserved selective marker of mammalian cells homologous to mouse CD8alpha+ dendritic cells. *The Journal of experimental medicine*. **207**, 1283–92 (2010).

11. M. Haniffa, A. Shin, V. Bigley, N. McGovern, P. Teo, P. See, P. S. Wasan, X.-N. N. Wang, F. Malinarich, B. Malleret, A. Larbi, P. Tan, H. Zhao, M. Poidinger, S. Pagan, S. Cookson, R. Dickinson, I. Dimmick, R. F. Jarrett, L. Renia, J. Tam, C. Song, J. Connolly, J. K. Chan, A. Gehring, A. Bertoletti, M. Collin, F. Ginhoux, Human tissues contain CD141hi cross-presenting dendritic cells with functional homology to mouse CD103+ nonlymphoid dendritic cells. *Immunity*. **37**, 60–73 (2012).

12. S. L. Jongbloed, A. J. Kassianos, K. J. McDonald, G. J. Clark, X. Ju, C. E. Angel, C.-J. J. Chen, P. R. Dunbar, R. B. Wadley, V. Jeet, A. J. Vulink, D. N. Hart, K. J. Radford, Human CD141+ (BDCA-3)+ dendritic cells (DCs) represent a unique myeloid DC subset that cross-presents necrotic cell antigens. *The Journal of experimental medicine*. **207**, 1247–60 (2010).

13. L. Poulin, M. Salio, E. Griessinger, F. Anjos-Afonso, L. Craciun, J.-L. Chen, A. M. Keller, O. Joffre, S. Zelenay, E. Nye, A. Moine, F. Faure, V. Donckier, D. Sancho, V. Cerundolo, D. Bonnet, C. e Sousa, Characterization of human DNGR-1+ BDCA3+ leukocytes as putative equivalents of mouse CD8α+ dendritic cells. *The Journal of Experimental Medicine*. **207**, 1261–1271 (2010).

14. F. Deauvieau, V. Ollion, A.-C. C. Doffin, C. Achard, J.-F. F. Fonteneau, E. Verronese, I. Durand, R. Ghittoni, J. Marvel, C. Dezutter-Dambuyant, T. Walzer, H. Vie, I. Perrot, N. Goutagny, C. Caux, J. Valladeau-Guilemond, Human natural killer cells promote cross-presentation of tumor

cell-derived antigens by dendritic cells. *International journal of cancer*. **136**, 1085–94 (2015).

15. M. Hubert, E. Gobbini, N. Bendriss-Vermare, C. Caux, J. Valladeau-Guilemond, Human Tumor-Infiltrating Dendritic Cells: From in Situ Visualization to High-Dimensional Analyses. *Cancers*. **11**, 1082 (2019).

16. D. Laoui, J. Keirsse, Y. Morias, E. V. Overmeire, X. Geeraerts, Y. Elkrim, M. Kiss, E. Bolli, Q. Lahmar, D. Sichien, J. Serneels, C. L. Scott, L. Boon, P. D. Baetselier, M. Mazzone, M. Guilliams, J. A. V. Ginderachter, The tumour microenvironment harbours ontogenically distinct dendritic cell populations with opposing effects on tumour immunity. *Nature communications*. **7**, 13720 (2016).

17. Y. Lavin, S. Kobayashi, A. Leader, E.-A. D. Amir, N. Elefant, C. Bigenwald, R. Remark, R. Sweeney, C. D. Becker, J. H. Levine, K. Meinhof, A. Chow, S. Kim-Shulze, A. Wolf, C. Medaglia, H. Li, J. A. Rytlewski, R. O. Emerson, A. Solovyov, B. D. Greenbaum, C. Sanders, M. Vignali, M. B. Beasley, R. Flores, S. Gnjatic, D. Pe'er, A. Rahman, I. Amit, M. Merad, Innate Immune Landscape in Early Lung Adenocarcinoma by Paired Single-Cell Analyses. *Cell*. **169**, 750–765.e17 (2017).

18. R. Zilionis, C. Engblom, C. Pfirschke, V. Savova, D. Zemmour, H. D. Saatcioglu, I. Krishnan, G. Maroni, C. V. Meyerovitz, C. M. Kerwin, S. Choi, W. G. Richards, A. D. Rienzo, D. G. Tenen, R. Bueno, E. Levantini, M. J. Pittet, A. M. Klein, Single-Cell Transcriptomics of Human and Mouse Lung Cancers Reveals Conserved Myeloid Populations across Individuals and Species. *Immunity* (2019).

19. K. C. Barry, J. Hsu, M. L. Broz, F. J. Cueto, M. Binnewies, A. J. Combes, A. E. Nelson, K. Loo, R. Kumar, M. D. Rosenblum, M. D. Alvarado, D. M. Wolf, D. Bogunovic, N. Bhardwaj, A. I. Daud, P. K. Ha, W. R. Ryan, J. L. Pollack, B. Samad, S. Asthana, V. Chan, M. F. Krummel, A natural killer-dendritic cell axis defines checkpoint therapy-responsive tumor microenvironments. *Nature medicine*. **24**, 1178–1191 (2018).

20. P. Michea, F. Noël, E. Zakine, U. Czerwinska, P. Sirven, O. Abouzid, C. Goudot, A. Scholer-Dahirel, A. Vincent-Salomon, F. Reyal, S. Amigorena, M. Guillot-Delost, E. Segura, V. Soumelis, Adjustment of dendritic cells to the breast-cancer microenvironment is subset specific. *Nature Immunology*. **19**, 885–897 (2018).

21. H. Lauterbach, B. Bathke, S. Gilles, C. Traidl-Hoffmann, C. A. Luber, G. Fejer, M. A. Freudenberg, G. M. Davey, D. Vremec, A. Kallies, L. Wu, K. Shortman, P. Chaplin, M. Suter, M. O'Keeffe, H. Hochrein, Mouse CD8α+ DCs and human BDCA3+ DCs are major producers of IFN-λ in response to poly IC. *The Journal of Experimental Medicine*. **207**, 2703–2717 (2010).

22. S. Balan, V. Ollion, N. Colletti, R. Chelbi, F. Montanana-Sanchis, H. Liu, T.-P. P. V. Manh, C. Sanchez, J. Savoret, I. Perrot, A.-C. C. Doffin, E. Fossum, D. Bechlian, C. Chabannon, B. Bogen, C. Asselin-Paturel, M. Shaw, T. Soos, C. Caux, J. Valladeau-Guilemond, M. Dalod, Human XCR1+ dendritic cells derived in vitro from CD34+ progenitors closely resemble blood dendritic cells, including their adjuvant responsiveness, contrary to monocyte-derived dendritic cells. *Journal of immunology (Baltimore, Md. : 1950)*. **193**, 1622–35 (2014).

23. L. Rönnblom, M.-L. Eloranta, The interferon signature in autoimmune diseases. *Current Opinion in Rheumatology*. **25**, 248–253 (2013).

24. P. Hermant, T. Michiels, Interferon-λ in the Context of Viral Infections: Production, Response and Therapeutic Implications. *Journal of Innate Immunity*. **6**, 563–574 (2014).

25. A. Lasfar, A. Lewis-Antes, S. V. Smirnov, S. Anantha, W. Abushahba, B. Tian, K. Reuhl, H. Dickensheets, F. Sheikh, R. P. Donnelly, E. Raveche, S. V. Kotenko, Characterization of the mouse IFN-lambda ligand-receptor system: IFN-lambdas exhibit antitumor activity against B16 melanoma. *Cancer research*. **66**, 4468–77 (2006).

26. A. Sato, M. Ohtsuki, M. Hata, E. Kobayashi, T. Murakami, Antitumor activity of IFN-lambda in murine tumor models. *Journal of immunology (Baltimore, Md. : 1950)*. **176**, 7686–94 (2006).

27. M. Numasaki, M. Tagawa, F. Iwata, T. Suzuki, A. Nakamura, M. Okada, Y. Iwakura, S. Aiba, M. Yamaya, IL-28 elicits antitumor responses against murine fibrosarcoma. *Journal of immunology (Baltimore, Md. : 1950)*. **178**, 5086–98 (2007).

28. W. Abushahba, M. Balan, I. Castaneda, Y. Yuan, K. Reuhl, E. Raveche, A. de la Torre, A. Lasfar, S. V. Kotenko, Antitumor activity of type I and type III interferons in BNL hepatoma model. *Cancer immunology, immunotherapy : CII*. **59**, 1059–71 (2010).

29. L. Dumoutier, A. Tounsi, T. Michiels, C. Sommereyns, S. V. Kotenko, J.-C. C. Renauld, Role of the interleukin (IL)-28 receptor tyrosine residues for antiviral and antiproliferative activity of IL-29/interferon-lambda 1: similarities with type I interferon signaling. *The Journal of biological chemistry*. **279**, 32269–74 (2004).

30. A. Meager, K. Visvalingam, P. Dilger, D. Bryan, M. Wadhwa, Biological activity of interleukins-28 and -29: comparison with type I interferons. *Cytokine*. **31**, 109–18 (2005).

31. W. Li, A. Lewis-Antes, J. Huang, M. Balan, S. V. Kotenko, Regulation of apoptosis by type III interferons. *Cell Proliferation*. **41**, 960–979 (2008).

32. Q. Li, K. Kawamura, G. Ma, F. Iwata, M. Numasaki, N. Suzuki, H. Shimada, M. Tagawa, Interferon-λ induces G1 phase arrest or apoptosis in oesophageal carcinoma cells and produces anti-tumour effects in combination with anti-cancer agents. *European Journal of Cancer*. **46**, 180–190 (2010).

33. M. Guilliams, F. Ginhoux, C. Jakubzick, S. H. Naik, N. Onai, B. U. Schraml, E. Segura, R. Tussiwand, S. Yona, Dendritic cells, monocytes and macrophages: a unified nomenclature based on ontogeny. *Nature reviews. Immunology*. **14**, 571–8 (2014).

34. A. Barclay, T. K. den Berg, The interaction between signal regulatory protein alpha (SIRPα) and CD47: structure, function, and therapeutic target. *Annual review of immunology*. **32**, 25–50 (2014).

35. S. H. Robbins, T. Walzer, D. Dembélé, C. Thibault, A. Defays, G. Bessou, H. Xu, E. Vivier, M. Sellars, P. Pierre, F. R. Sharp, S. Chan, P. Kastner, M. Dalod, Novel insights into the relationships between dendritic cell subsets in human and mouse revealed by genome-wide expression profiling. *Genome biology*. **9**, R17 (2008).

36. M. Binnewies, A. M. Mujal, J. L. Pollack, A. J. Combes, E. A. Hardison, K. C. Barry, J. Tsui, M. K. Ruhland, K. Kersten, M. A. Abushawish, M. Spasic, J. P. Giurintano, V. Chan, A. I. Daud, P. Ha, C. J. Ye, E. W. Roberts, M. F. Krummel, Unleashing Type-2 Dendritic Cells to Drive Protective Antitumor CD4+ T Cell Immunity. *Cell*. **177**, 556–571.e16 (2019).

37. A.-C. Villani, R. Satija, G. Reynolds, S. Sarkizova, K. Shekhar, J. Fletcher, M. Griesbeck, A. Butler, S. Zheng, S. Lazo, L. Jardine, D. Dixon, E. Stephenson, E. Nilsson, I. Grundberg, D. McDonald, A. Filby, W. Li, P. L. D. Jager, O. Rozenblatt-Rosen, A. A. Lane, M. Haniffa, A. Regev, N. Hacohen, Single-cell RNA-seq reveals new types of human blood dendritic cells, monocytes, and progenitors. *Science*. **356**, eaah4573 (2017).

38. K. Tomczak, P. Czerwińska, M. Wiznerowicz, The Cancer Genome Atlas (TCGA): an immeasurable source of knowledge. *Contemporary oncology (Poznan, Poland)*. **19**, A68–77 (2015).

39. E. Becht, N. A. Giraldo, L. Lacroix, B. Buttard, N. Elarouci, F. Petitprez, J. Selves, P. Laurent-Puig, C. Sautès-Fridman, W. H. Fridman, A. de Reyniès, Estimating the population abundance of tissue-infiltrating immune and stromal cell populations using gene expression. *Genome biology*. **17**, 218 (2016).

40. L. Spinelli, S. Carpentier, F. M. Sanchis, M. Dalod, T.-P. P. V. Manh, BubbleGUM: automatic extraction of phenotype molecular signatures and comprehensive visualization of multiple Gene Set Enrichment Analyses. *BMC genomics*. **16**, 814 (2015).

41. V. Sisirak, J. Faget, M. Gobert, N. Goutagny, N. Vey, I. Treilleux, S. Renaudineau, G. Poyet, S. I. Labidi-Galy, S. Goddard-Leon, I. Durand, I. Mercier, A. Bajard, T. Bachelot, A. Puisieux, I. Puisieux, J.-Y. Y. Blay, C. Ménétrier-Caux, C. Caux, N. Bendriss-Vermare, Impaired IFN-α production by plasmacytoid dendritic cells favors regulatory T-cell expansion that may contribute to breast cancer progression. *Cancer research*. **72**, 5188–97 (2012).

42. N. Ank, M. B. Iversen, C. Bartholdy, P. Staeheli, R. Hartmann, U. B. Jensen, F. Dagnaes-Hansen, A. R. Thomsen, Z. Chen, H. Haugen, K. Klucher, S. R. Paludan, An important role for type III interferon (IFN-lambda/IL-28) in TLR-induced antiviral activity. *Journal of immunology (Baltimore, Md. : 1950)*. **180**, 2474–85 (2008).

43. S. V. Kotenko, G. Gallagher, V. V. Baurin, A. Lewis-Antes, M. Shen, N. K. Shah, J. A. Langer, F. Sheikh, H. Dickensheets, R. P. Donnelly, IFN-λs mediate antiviral protection through a distinct class II cytokine receptor complex. *Nature Immunology*. **4**, 6977 (2002).

44. S. Zhang, K. Kodys, K. Li, G. Szabo, Human type 2 myeloid dendritic cells produce interferon-λ and amplify interferon-α in response to hepatitis C virus infection. *Gastroenterology*. **144**, 414–425.e7 (2013).

45. L. Ye, D. Schnepf, P. Staeheli, Interferon-λ orchestrates innate and adaptive mucosal immune responses. *Nature Reviews Immunology*. **19**, 614–625 (2019).

46. K. B. Chiappinelli, P. L. Strissel, A. Desrichard, H. Li, C. Henke, B. Akman, A. Hein, N. S. Rote, L. M. Cope, A. Snyder, V. Makarov, S. Budhu, D. J. Slamon, J. D. Wolchok, D. M. Pardoll, M. W. Beckmann, C. A. Zahnow, T. Merghoub, T. A. Chan, S. B. Baylin, R. Strick, Inhibiting DNA Methylation Causes an Interferon Response in Cancer via dsRNA Including Endogenous Retroviruses. *Cell*. **164**, 1073

(2016).

47. H. Sui, M. Zhou, H. Imamichi, X. Jiao, B. T. Sherman, H. C. Lane, T. Imamichi, STING is an essential mediator of the Ku70-mediated production of IFN-λ1 in response to exogenous DNA. *Sci. Signal.* **10**, eaah5054 (2017).

48. M. Wendel, I. E. Galani, E. Suri-Payer, A. Cerwenka, Natural Killer Cell Accumulation in Tumors Is Dependent on IFN-γ and CXCR3 Ligands. *Cancer Research*. **68**, 8437–8445 (2008).

49. R. Tokunaga, W. Zhang, M. Naseem, A. Puccini, M. D. Berger, S. Soni, M. McSkane, H. Baba, H.-J. Lenz, CXCL9, CXCL10, CXCL11/CXCR3 axis for immune activation – A target for novel cancer therapy. *Cancer Treatment Reviews*. **63**, 40–47 (2018).

50. J. P. Böttcher, M. Beyer, F. Meissner, Z. Abdullah, J. Sander, B. Höchst, S. Eickhoff, J. C. Rieckmann, C. Russo, T. Bauer, T. Flecken, D. Giesen, D. Engel, S. Jung, D. H. Busch, U. Protzer, R. Thimme, M. Mann, C. Kurts, J. L. Schultze, W. Kastenmüller, P. A. Knolle, Functional classification of memory CD8+ T cells by CX3CR1 expression. *Nature Communications*. **6**, 8306 (2015).

51. H. M. Lazear, J. W. Schoggins, M. S. Diamond, Shared and Distinct Functions of Type I and Type III Interferons. *Immunity*. **50**, 907–923 (2019).

52. D. P. Simmons, P. A. Wearsch, D. H. Canaday, H. J. Meyerson, Y. C. Liu, Y. Wang, W. Boom, C. V. Harding, Type I IFN drives a distinctive dendritic cell maturation phenotype that allows continued class II MHC synthesis and antigen processing. *Journal of immunology (Baltimore, Md. : 1950)*. **188**, 3116–26 (2012).

53. M. B. Fuertes, A. K. Kacha, J. Kline, S.-R. R. Woo, D. M. Kranz, K. M. Murphy, T. F. Gajewski, Host type I IFN signals are required for antitumor CD8+ T cell responses through CD8{alpha}+ dendritic cells. *The Journal of experimental medicine*. **208**, 2005–16 (2011).

54. F. Souza-Fonseca-Guimaraes, A. Young, D. Mittal, L. Martinet, C. Bruedigam, K. Takeda, C. E. Andoniou, M. A. Degli-Esposti, G. R. Hill, M. J. Smyth, NK cells require IL-28R for optimal in vivo activity. *Proceedings of the National Academy of Sciences of the United States of America*. **112**, E2376–84 (2015).

55. G. Gautier, M. Humbert, F. Deauvieau, M. Scuiller, J. Hiscott, E. E. M. Bates, G. Trinchieri, C. Caux, P. Garrone, A type I interferon autocrine–paracrine loop is involved in Toll-like receptor-induced interleukin-12p70 secretion by dendritic cells. *The Journal of Experimental Medicine*. **201**, 1435–1446 (2005).

56. R. A. de Groen, Z. M. Groothuismink, B.-S. S. Liu, A. Boonstra, IFN-λ is able to augment TLR-mediated activation and subsequent function of primary human B cells. *Journal of leukocyte biology*. **98**, 623–30 (2015).

57. G. Finotti, N. Tamassia, M. A. Cassatella, Interferon-λs and Plasmacytoid Dendritic Cells: A Close Relationship. *Frontiers in Immunology*. **8**, 1015 (2017).

58. N. J. Megjugorac, G. E. Gallagher, G. Gallagher, IL-4 enhances IFN-lambda1 (IL-29) production by plasmacytoid DCs via monocyte secretion of IL-1Ra. *Blood*. **115**, 4185–90 (2010).

59. F. Liu, C. Liu, X. Hu, Y. Shang, L. Wu, MicroRNA-21: A Positive Regulator for Optimal Production of Type I and Type III Interferon by Plasmacytoid Dendritic Cells. *Frontiers in Immunology*. **8**, 947 (2017).

60. A. Kelly, M. W. Robinson, G. Roche, C. A. Biron, C. O'Farrelly, E. J. Ryan, Immune Cell Profiling of IFN-λ Response Shows pDCs Express Highest Level of IFN-λR1 and Are Directly Responsive Via the JAK-STAT Pathway. *Journal of interferon & cytokine research : the official journal of the International Society for Interferon and Cytokine Research* (2016), doi:10.1089/jir.2015.0169.

61. G. Finotti, N. Tamassia, F. Calzetti, G. Fattovich, M. A. Cassatella, Endogenously produced TNF-α contributes to the expression of CXCL10/IP-10 in IFN-λ3-activated plasmacytoid dendritic cells. *Journal of Leukocyte Biology*. **99**, 107–119 (2016).

62. G. Finotti, N. Tamassia, M. A. Cassatella, Synergistic production of TNFα and IFNα by human pDCs incubated with IFNλ3 and IL-3. *Cytokine*. **86**, 124–131 (2016).

63. C. Liu, Y. Lou, G. Lizée, H. Qin, S. Liu, B. Rabinovich, G. J. Kim, Y.-H. H. Wang, Y. Ye, A. G. Sikora, W. W. Overwijk, Y.-J. J. Liu, G. Wang, P. Hwu, Plasmacytoid dendritic cells induce NK cell-dependent, tumor antigen-specific T cell cross-priming and tumor regression in mice. *The Journal of clinical investigation*. **118**, 1165–75 (2008).

64. T. A. Selvakumar, S. Bhushal, U. Kalinke, D. Wirth, H. Hauser, M. Köster, M. W. Hornef, Identification of a Predominantly Interferon-λ-Induced Transcriptional Profile in Murine Intestinal Epithelial Cells. *Frontiers in immunology*. **8**, 1302 (2017).

65. S. Ding, W. Khoury-Hanold, A. Iwasaki, M. D. Robek, Epigenetic reprogramming of the type III interferon response potentiates antiviral activity and suppresses tumor growth. *PLoS biology*. **12**, e1001758 (2014).

66. D. Bell, P. Chomarat, D. Broyles, G. Netto, G. M. Harb, S. Lebecque, J. Valladeau, J. Davoust, K. A. Palucka, J. Banchereau, In breast carcinoma tissue, immature dendritic cells reside within the tumor, whereas mature dendritic cells are located in peritumoral areas. *The Journal of experimental medicine*. **190**, 1417–26 (1999).

67. J. Faget, N. Bendriss-Vermare, M. Gobert, I. Durand, D. Olive, C. Biota, T. Bachelot, I. Treilleux, S. Goddard-Leon, E. Lavergne, S. Chabaud, J. Y. Blay, C. Caux, C. Ménétrier-Caux, ICOS-ligand expression on plasmacytoid dendritic cells supports breast cancer progression by promoting the accumulation of immunosuppressive CD4+ T cells. *Cancer research*. **72**, 6130–41 (2012).

68. D. Howie, S. P. Cobbold, E. Adams, A. T. Bokum, A. S. Necula, W. Zhang, H. Huang, D. J. Roberts, B. Thomas, S. S. Hester, D. J. Vaux, A. G. Betz, H. Waldmann, Foxp3 drives oxidative phosphorylation and protection from lipotoxicity. *JCI Insight*. **2**, e89160 (2017).

69. S. Terry, P. Savagner, S. Ortiz-Cuaran, L. Mahjoubi, P. Saintigny, J. Thiery, S. Chouaib, New insights into the role of EMT in tumor immune escape. *Molecular Oncology*. **11**, 824–846 (2017).

70. S. I. Labidi-Galy, V. Sisirak, P. Meeus, M. Gobert, I. Treilleux, A. Bajard, J.-D. D. Combes, J. Faget, F. Mithieux, A. Cassignol, O. Tredan, I. Durand, C. Ménétrier-Caux, C. Caux, J.-Y. Y. Blay, I. Ray-Coquard, N. Bendriss-Vermare, Quantitative and functional alterations of plasmacytoid dendritic cells contribute to immune tolerance in ovarian cancer. *Cancer research*. **71**, 5423–34 (2011).

71. Y. Wu, X. Wu, L. Wu, X. Wang, Z. Liu, The anticancer functions of RIG-I-like receptors, RIG-I and MDA5, and their applications in cancer therapy. *Transl Res*. **190**, 51–60 (2017).

72. E. D. l-AD Amir, K. L. Davis, M. D. Tadmor, E. F. Simonds, J. H. Levine, S. C. Bendall, D. K. Shenfeld, S. Krishnaswamy, G. P. Nolan, D. Pe'er, viSNE enables visualization of high dimensional single-cell data and reveals phenotypic heterogeneity of leukemia. *Nature biotechnology*. **31**, 545–52 (2013).

73. A. M. Szász, A. Lánczky, Á. Nagy, S. Förster, K. Hark, J. E. Green, A. Boussioutas, R. Busuttil, A. Szabó, B. Győrffy, Cross-validation of survival associated biomarkers in gastric cancer using transcriptomic data of 1,065 patients. *Oncotarget*. **7**, 49322–49333 (2016).

74. A. Subramanian, P. Tamayo, V. K. Mootha, S. Mukherjee, B. L. Ebert, M. A. Gillette, A. Paulovich, S. L. Pomeroy, T. R. Golub, E. S. Lander, J. P. Mesirov, Gene set enrichment analysis: A knowledge-based approach for interpreting genome-wide expression profiles. *Proceedings of the National Academy of Sciences of the United States of America*. **102**, 15545–15550 (2005).

Acknowledgments:

We wish to thank the staff of the core facilities at the Cancer Research Center of Lyon (CRCL) for their technical assistance and the BRC (Biological Resources Centre) of the CLB (Centre Léon Bérard) for providing human samples, as well as N. Gadot and the research anatomophalogy plateform of the CLB. We are very grateful to S. Leon and the *Ex Vivo* platform (Department of Translationnal Research and Innovation of the CLB, Lyon, France) for their precious help on thick tumor slice analysis. We thank I. Durand and P. Battiston-Montagne for their assistance for flow cytometry and T. Andrieu for viSNE analyses. We would also like to thank Dr. B. Manship for critical reading of the manuscript.

Fundings:

This work was supported by funding from INSERM, INCA (PLBIO INCa_4508 and PLBIO INCa_11155), ANRS, ARC, Ligue contre le Cancer (Régionale Auvergne-Rhône-Alpes et Saône-et-Loire, Comité de la Savoie), and la Région Rhône-Alpes Auvergne (IRICE). We would like to thank our financial supports: the Région Auvergne-Rhône-Alpes and the ARC Foundation for M. Hubert, the ESMO for E. Gobbini (any views, opinions, findings, conlusions or recommendations expressed in this material are those solely of the authors and do not necessarily reflect those of ESMO), SIRIC project (LYRIC, grant no. INCa_4664) and the FP7 European TumAdoR project (grant no. 602200) for C. Rodriguez and C. Caux, the LABEX DEVweCAN (ANR-10-LABX-0061) of the University of Lyon, within the program “Investissements d'Avenir” organized by the French National Research Agency (ANR), for V. Ollion, A.C. Doffin, N. Bendriss-Vermare, C. Caux and J. Valladeau-Guilemond.

Author contributions

M.H. designed and performed experiments and bioinformatics, analyzed results, did statistical analysis and wrote the manuscript. E.G, C.Co., A.C.D, C.R., V.O., and C.S. performed experiments and analyzed results. J.B. and B.D. set up a pipeline for the quantification of *in situ* stainings. T.P.V.M. and J.K. performed bioinformatics and wrote the manuscript; I.T. and O.T. contributed to clinical project management, pathology review and provided clinical samples. M.D., N.B.V. and C.Ca. provided strategic advice and revised the manuscript. J.V.G. designed experiments, supervised the research and wrote the manuscript.

Competing interests:

The authors declare that they have no competing interests.

Figure legends

Fig. 1 cDC1 infiltrate human breast tumors. (A) FACS gating strategy allowing the identification of four TA-DC subsets among viable $CD45^+$ $HLA\text{-}DR^+$ $Lineage^-$ (CD3/14/15/19/56) populations, namely: pDCs ($CD11c^-$ $CD123^+$), cDC1 ($CD11c^+$ $BDCA1^-$ $BDCA3^{hi}$), cDC2 ($CD11c^+$ $BDCA1^+$ $BDCA3^{-/low}$ $CD207^-$) and LCs ($CD11c^+$ $BDCA1^+$ $BDCA3^{-/low}$ $CD207^{hi}$). Representative results of n = 21 breast tumors. **(B)** Phenotypic characterization of TA-DC subsets for indicated markers by FACS. Color histogram = indicated marker, dotted line = isotype control. Representative results of n > 8 breast tumors. **(C)** viSNE analysis of viable $CD45^+$ $HLA\text{-}DR^+$ Lin^- for the expression of CD11c, CD123, BDCA1, BDCA3, CD207, CLEC9A, CD11b, SIRP-α and BTLA markers, color-coded according to the relative expression of markers (top), with populations indicated. Representative result of n = 4 breast tumors.

Fig. 2 cDC1 are the only DC subset enriched in breast tumors compared with patient PBMCs. (A-B) Proportion of each TA-DC subset (identified with the gating strategy defined in Figure 1) among viable $CD45^+$ cells in n = 23 patient PBMCs **(A)** and in n=21 breast tumors **(B)**. Statistical analysis by Friedman test. **(C)** Ratio of one DC subset to all DCs among viable $CD45^+$ cells. Statistical analysis: Mann-Whitney test. Horizontal bars represent the median of each group of samples. *p<0.05, **p<0.01, ***p<0.001, ***p<0.0001.

Fig. 3 TA-cDC1 are strongly associated with an increased overall survival in multiple human cancers. (A) Kaplan-Meier analysis of the overall survival of patients stratified according to the median for the expression score of each DC subset infiltrating breast tumors (calculated with the MCP-counter algorithm) using TCGA data sets. Statistical analysis: log rank test. **(B)** Summary of p values associated with the log rank test evaluating the prognostic impact of each DC subset in 14 human TCGA cancer data sets.

Fig. 4 Enrichment of IFN signatures is a specific feature of cDC1-infiltrated tumors. (A) Visualization of $CD8^+$ T cells and cDC1 respectively by *CD8A* (green) and *CLEC9A* (red) probes *in situ* hybridization, combined to an opal-based immunofluorescent staining of cytokeratin-positive tumor cells (white). Nuclei were counterstained with DAPI. White scale bars represent 50 µm for 40X images and 25 µm for 100X images. **(B)** Quantification of *CD8*$^+$ T cells and *CLEC9A*$^+$ cDC1 in 8 breast tumors using the Halo software.

Pearson correlation test. **(C)** Proportion of both cDC1 in stroma *versus* tumor bed, and of cDC1 in close contact with at least one $CD8^+$ T cell, quantified with the Halo software. **(D)** Scatterplots showing the Spearman correlation between $CD8^+$ T cell and each TA-DC subset scores (calculated with the MCP-counter algorithm) in n = 1100 breast tumors (TCGA data sets). **(E)** High-throughput GSEA analysis by BubbleGUM in breast tumors enriched in only one DC subset (TCGA data set, n = 48 for cDC1, n = 18 for cDC2, n = 95 for LCs and n = 67 for pDCs). Bubble enrichment patterns (black boxes) highlighted by the selection of gene sets (from Hallmark collection (H) or homemade gene sets) and pairwise comparisons of interest. **(F)** Heatmaps illustrating genes extracted from the overlap of the GSEA leading edges identified by each pairwise comparison between breast tumors enriched only in cDC1 and those enriched only in one of the 3 other DC subsets. Gene expression values were averaged across tumors enriched in only one DC subset and then log2-transformed.

Fig. 5 IFN-λ1 is specifically produced by cDC1 in breast tumors. (A) Differential expression analysis of the *IFNL1* gene in multiple transcriptomic TCGA data sets between the tumor (gray boxes) and the normal adjacent tissue (white boxes). Statistical analysis: Wilcoxon test. **(B)** IFN-λ1 quantification by ECLIA multiplex assay in n = 107 STMs of human breast tumors. **(C)** Intracellular IFN-λ1 FACS staining of one representative breast tumor suspension positive for IFN-λ1 (grey contour plot = isotype control). **(D)** Proportion of IFN-λ1 producing cells in n = 12 breast tumor suspensions. Horizontal bars represent the median of each group of samples. **(E)** *In situ* detection of IFN-λ1 producing cells: *CLEC9A* (red) and *IFNL1* (green) mRNA were stained by duplex RNAscope, combined to an opal-based immunofluorescent staining of cytokeratin-positive tumor cells (white). Nuclei were counterstained with DAPI. White scale bars represent 50 µm for 40X images and 25 µm for 100X images. **(F-G)** Quantification of *IFNL1* and *CLEC9A* simple and double positive cells in 16 randomly-selected zones of 0.64 mm2 per tumor using the Halo software in 6 breast tumors. The mean for each tumor is represented in **(F)** and the exact quantification of the 2/6 $IFNL1^+$ tumors (#01 and #03) in **(G)**. Bars and error bars respectively represent the mean and the SEM for each group of samples. Statistical analysis: Friedman test. *p<0.05, **p<0.01, ***p<0.001, ***p<0.0001.

Fig. 6 IFN-λ1 is associated with a favorable outcome and with a Th1 tumor microenvironment in breast cancer. (A) Kaplan-Meier analysis of the relapse-free survival of patients stratified according to the median for the expression of *IFNL1* and *IFNLR1* genes (KMplot transcriptomic data sets). Statistical analysis by log

rank test. **(B)** Spearman correlation factors between IFN-λ1 and the other cytokines and chemokines quantified in n = 107 STMs of human breast tumors by ECLIA multiplex assay. **(C)** Cytokine and chemokine quantification by ECLIA multiplex in the supernatants of n = 6 tumor cell suspensions treated or not with IFN-λ1 for 24 h. Bars and error bars respectively represent the mean and the SEM for each group of samples. Statistical analysis: Paired t tests, *p<0.05, **p<0.01, ***p<0.001, ***p<0.0001.

Fig. 7 cDC1 activation by TLR3-L stimulated their IFN-λ1 production and the induction of Th1 immune responses. (A) Representative FACS plots of *ex vivo* IFN-λ1 production by DC subsets from patient PBMCs and breast tumor suspensions treated or not with TLR-L (PolyI:C + R848) for 5h. DC subsets were identified using the gating strategy defined in Fig. 1 and fig S1. **(B)** Proportion of IFN-λ1 and IFN-α producing DC subsets of n = 20 patient PBMCs and n = 12 fresh breast tumor suspensions treated or not with TLR-L (PolyI:C + R848) for 5 h. The medium condition corresponds to Fig. 5C. Bars and error bars respectively represent the mean and the SEM for each group of samples. Statistical analysis: Paired t test. **(C)** Multiplex quantification by ECLIA assay of cytokines and chemokines in the supernatants of n = 6 fresh tumor thick sections treated or not with TLR3-L (Poly(I:C)) for 48 h. Bars and error bars respectively represent the mean and the SEM for each group of samples. Statistical analysis: Wilcoxon test, *p<0.05, **p<0.01, ***p<0.001, ***p<0.0001.

Fig. S1. Identification of DC subsets in patient PBMCs. (A) FACS gating strategy allowing the identification of four DC subsets among viable $CD45^+$ $HLA\text{-}DR^+$ $Lineage^-$ (CD3/14/15/19/56) populations in patient PBMCs: pDCs ($CD11c^-$ $CD123^+$), cDC1 ($CD11c^+$ $BDCA1^-$ $BDCA3^{hi}$), cDC2 ($CD11c^+$ $BDCA1^+$ $BDCA3^{-/low}$ $CD207^-$) and LCs ($CD11c^+$ $BDCA1^+$ $BDCA3^{-/low}$ $CD207^{hi}$). Representative results of n = 10 patients. **(B)** Phenotypic characterization of TA-DC subsets for indicated markers by FACS. Color histogram = indicated marker, dotted line = isotype control. Representative results of n = 8 independent experiments. **(C)** viSNE analysis of viable $CD45^+$ $HLA\text{-}DR^+$ Lin^- for the expression of CD11c, CD123, BDCA1, BDCA3, CD207, CLEC9A, CD11b, SIRP-α and BTLA markers, color-coded for the relative expression of FACS markers, with populations indicated (top). Representative results of n = 4 independent experiments.

Fig. S2. Proportion of DCs among the immune infiltrate of breast tumors, (A) Proportion of $DC\text{-}LAMP^+$ cells among all TA-DC subsets analyzed by FACS. Statistical analysis: Kruskal-Wallis test. **(B)** Number of

$CD45^+$ infiltrating cells per milligram of n = 90 breast tumors. **(C-E)** Proportion of cDC1 **(C)**, $BDCA1^+$ DCs **(D)** and pDCs **(E)** (identified with the gating strategy defined in figure S1) among viable $CD45^+$ cells. This was done on different tumor types (TNBC, luminal and Her2 amplified) and grades (SBR1, 2 ,3) in n = 61 breast tumors for cDC1 and in n = 19 breast tumors for $BDCA1^+$ DCs and pDCs. Statistical analysis: Kruskal-Wallis test, Horizontal bars represent the median of each group of samples. *p<0.05, **p<0.01, ***p<0.001, ***p<0.0001.

Fig. S3. Kaplan-Meier analysis of the overall survival of cancer patients (Part 1 and 2). Patients were stratified according to the median expression score of each DC subset infiltrating in 13 human tumors (calculated with MCP-counter algorithm) using TCGA data sets. Statistical analysis: log rank test.

Fig. S4. *In silico* analysis of pathways associated to each DC infiltration score. (A) Enrichment plots of gene set enrichment analysis between "cDC1-enriched" breast tumors compared with "another DC subset-enriched" breast tumors. **(B)** Scatterplots showing the Spearman correlation between Tregs and each TA-DC subset scores (calculated with MCP-counter algorithm) in n = 1100 breast tumors (TCGA data sets).

Fig. S5. Quantification of IFNs in breast tumors. (A) Spearman correlation between IFN-λ1 and IFN-λ2 quantified in breast tumor supernatants by ECLIA multiplex assay. **(B)** IFN quantification by ECLIA multiplex assay in n = 107 STMs of human breast tumors. Statistical analysis by Friedman test. **(C)** IFN gene expression in the TCGA data set of breast cancer (n = 1090 patients). **(D)** *Ex vivo* intracellular IFN-α and TNF-α FACS staining in n = 12 fresh breast tumor suspensions without any stimulation. **(E)** Quantification of *CLEC9A* positive cells in n = 6 breast tumors using the Halo software. Bars and error bars respectively represent the mean and the SEM for each group of samples. Statistical analysis: Kruskal-Wallis test. *p<0.05, **p<0.01, ***p<0.001, ***p<0.0001.

Fig. S6. Correlations between the soluble factors present in human tumors. Heatmap of Spearman correlation coefficients between each cytokine and chemokine quantified in n = 107 STMs of human breast tumor by ECLIA.

Fig. S7. Analysis of the TNF-α production by DC subsets infiltrating breast tumors. Intracellular TNF-α FACS staining in n = 20 patient PBMCs and n = 12 fresh breast tumor suspensions treated or not with TLR-L (PolyI:C + R848) for 5 h. DC subsets were identified using the gating strategy defined in Fig. 1 and fig S1. Statistical analysis: Wilcoxon test, *p<0.05, **p<0.01, ***p<0.001, ***p<0.0001.

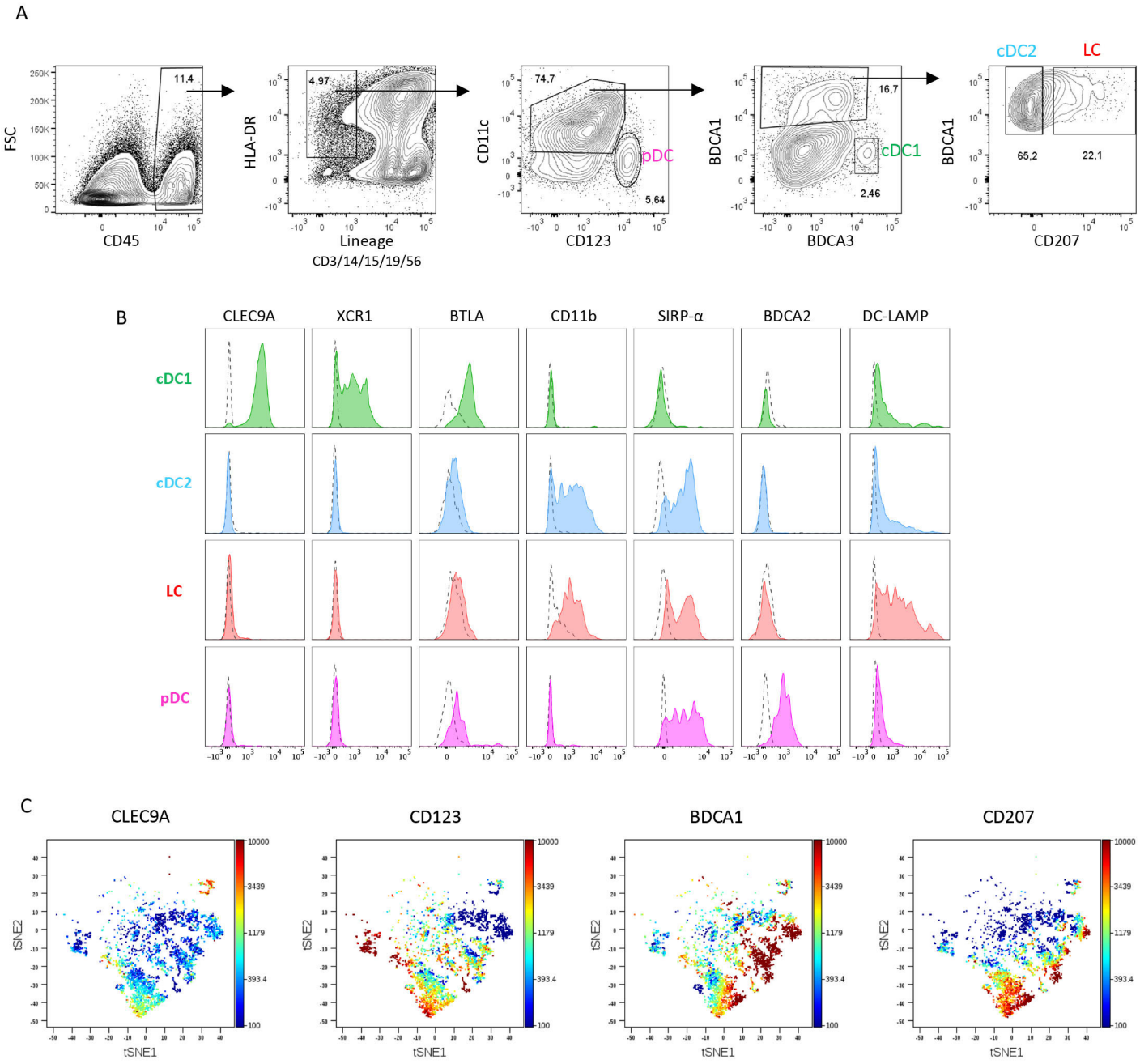

Fig. 1 cDC1 infiltrate human breast tumors. (A) FACS gating strategy allowing the identification of four TA-DC subsets among viable CD45^{+} HLA-DR^{+} Lineage^{-} (CD3/14/15/19/56) populations, namely: pDCs (CD11c^{-} CD123^{+}), cDC1 (CD11c^{+} BDCA1^{-} BDCA3^{hi}), cDC2 (CD11c^{+} BDCA1^{+} BDCA3$^{-/low}$ CD207^{-}) and LCs (CD11c^{+} BDCA1^{+} BDCA3$^{-/low}$ CD207^{hi}). Representative results of n = 21 breast tumors. **(B)** Phenotypic characterization of TA-DC subsets for indicated markers by FACS. Color histogram = indicated marker, dotted line = isotype control. Representative results of n > 8 breast tumors. **(C)** viSNE analysis of viable CD45^{+} HLA-DR^{+} Lin^{-} for the expression of CD11c, CD123, BDCA1, BDCA3, CD207, CLEC9A, CD11b, SIRP-α and BTLA markers, color-coded according to the relative expression of markers (top), with populations indicated. Representative result of n = 4 breast tumors.

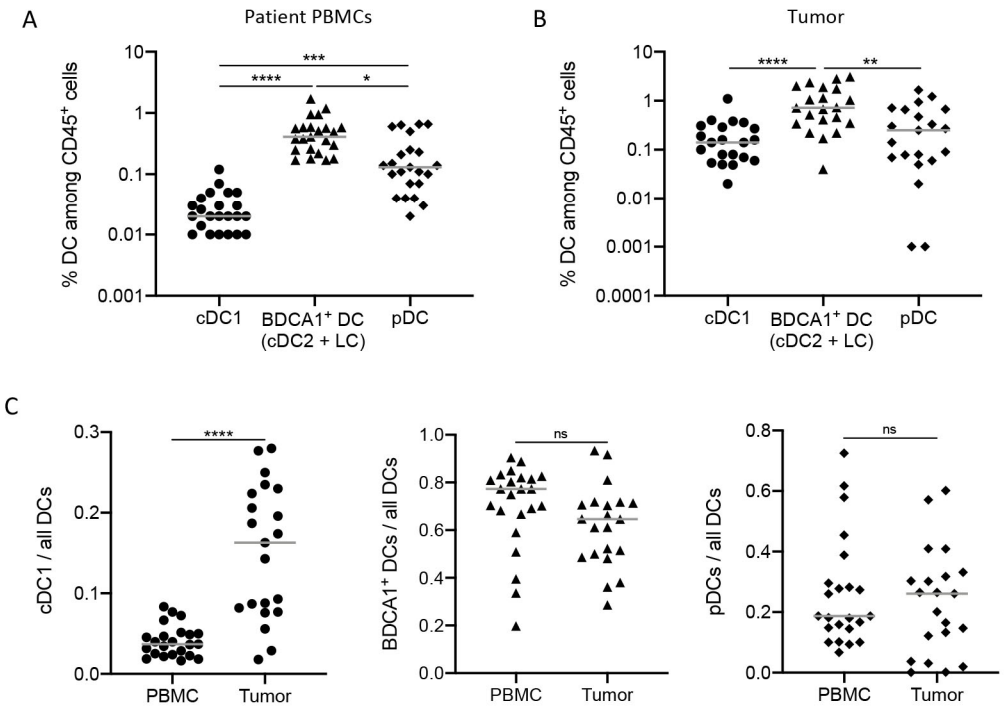

Fig. 2 cDC1 are the only DC subset enriched in breast tumors compared with patient PBMCs. (A-B) Proportion of each TA-DC subset (identified with the gating strategy defined in Figure 1) among viable $CD45^+$ cells in n = 23 patient PBMCs **(A)** and in n=21 breast tumors **(B)**. Statistical analysis by Friedman test. **(C)** Ratio of one DC subset to all DCs among viable $CD45^+$ cells. Statistical analysis: Mann-Whitney test. Horizontal bars represent the median of each group of samples. *p<0.05, **p<0.01, ***p<0.001, ***p<0.0001.

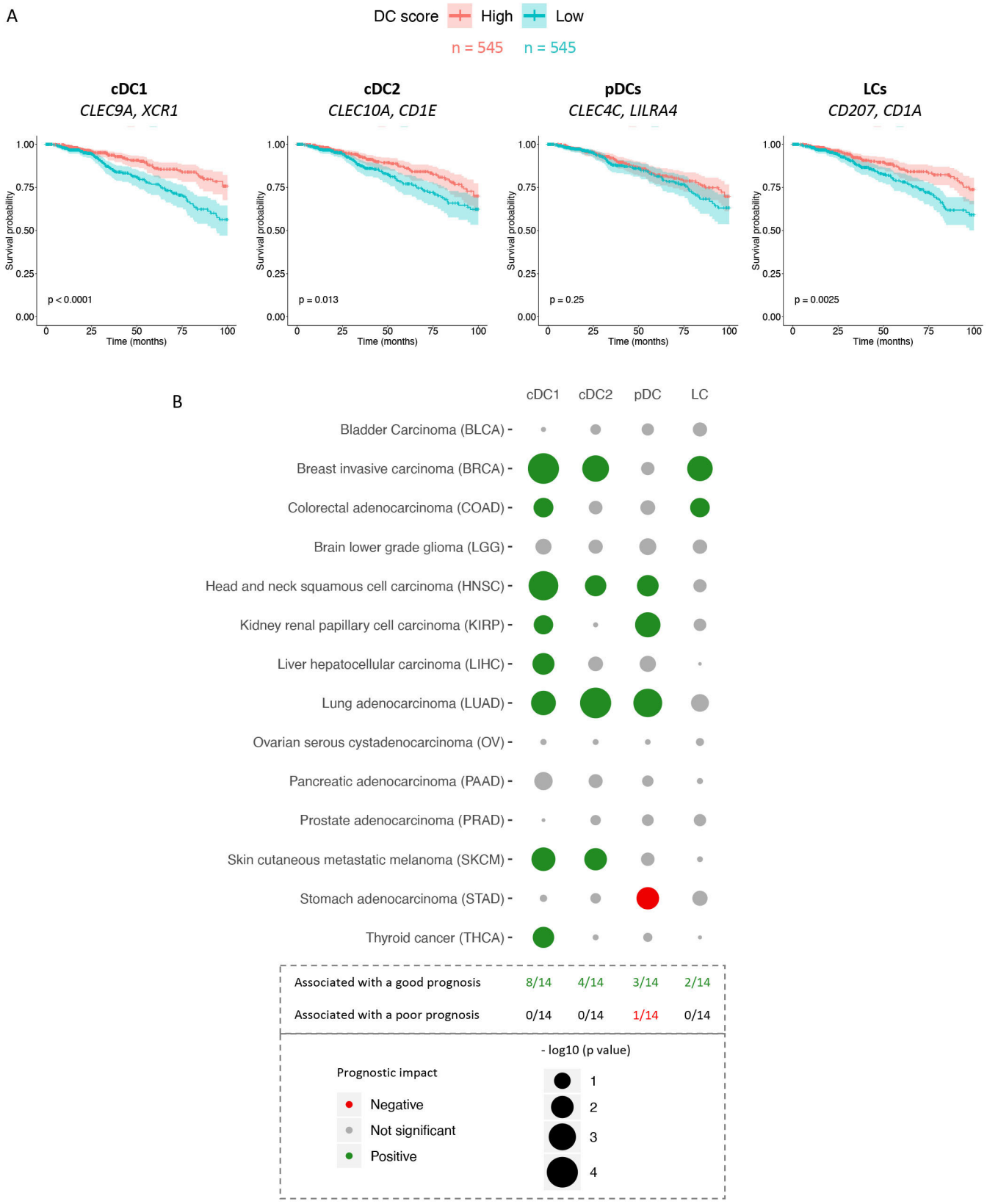

Fig. 3 TA-cDC1 are strongly associated with an increased overall survival in multiple human cancers. (A) Kaplan-Meier analysis of the overall survival of patients stratified according to the median for the expression score of each DC subset infiltrating breast tumors (calculated with the MCP-counter algorithm) using TCGA data sets. Statistical analysis: log rank test. **(B)** Summary of p values associated with the log rank test evaluating the prognostic impact of each DC subset in 14 human TCGA cancer data sets.

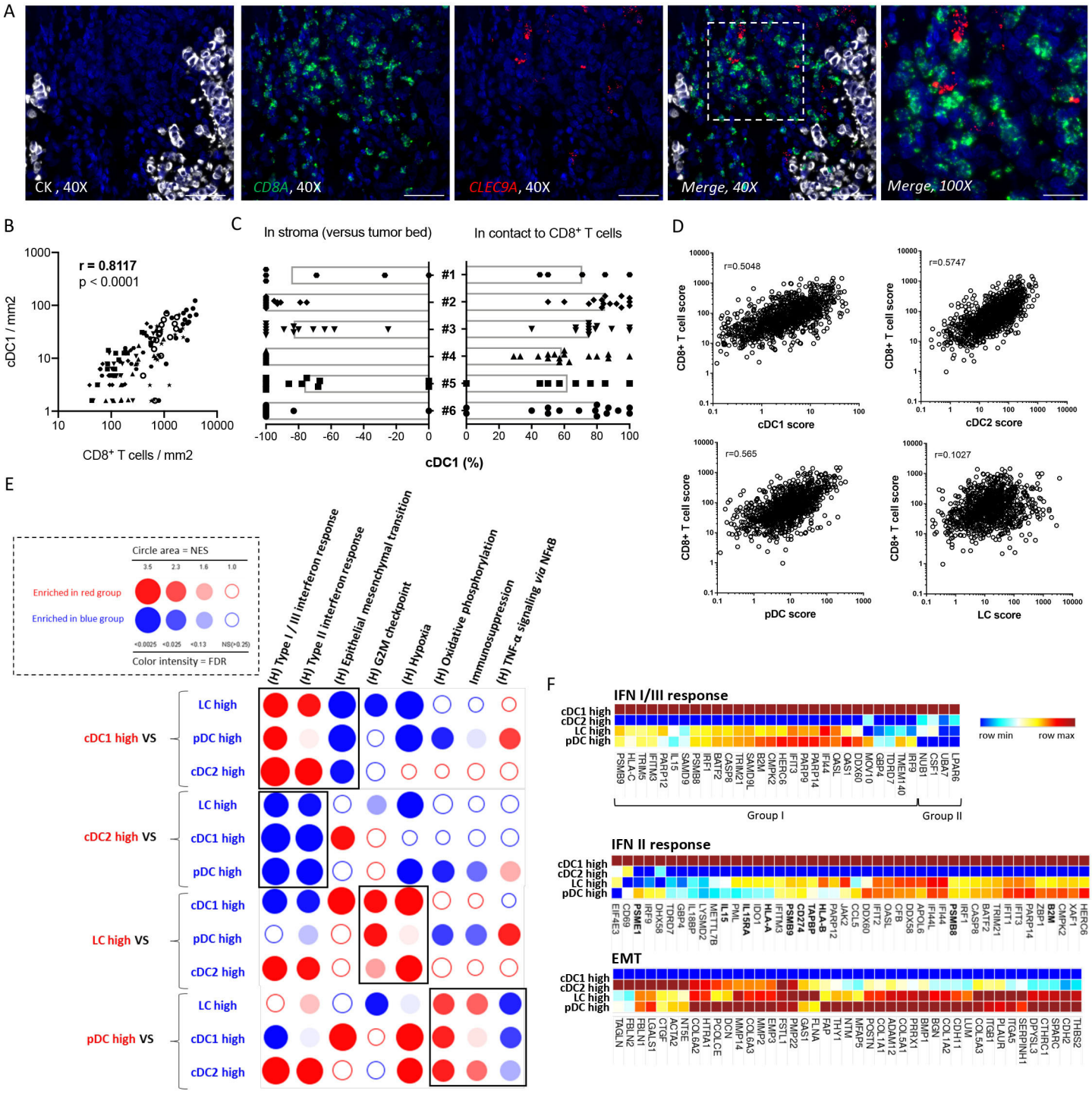

Fig. 4 Enrichment of IFN signatures is a specific feature of cDC1-infiltrated tumors. (A) Visualization of CD8⁺ T cells and cDC1 respectively by *CD8A* (green) and *CLEC9A* (red) probes *in situ* hybridization, combined to an opal-based immunofluorescent staining of cytokeratin-positive tumor cells (white). Nuclei were counterstained with DAPI. White scale bars represent 50 µm for 40X images and 25 µm for 100X images. **(B)** Quantification of *CD8*⁺ T cells and *CLEC9A*⁺ cDC1 in 8 breast tumors using the Halo software. Pearson correlation test. **(C)** Proportion of both cDC1 in stroma *versus* tumor bed, and of cDC1 in close contact with at least one CD8⁺ T cell, quantified with the Halo software. **(D)** Scatterplots showing the Spearman correlation between CD8⁺ T cell and each TA-DC subset scores (calculated with the MCP-counter algorithm) in n = 1100 breast tumors (TCGA data sets). **(E)** High-throughput GSEA analysis by BubbleGUM in breast tumors enriched in only one DC subset (TCGA data set, n = 48 for cDC1, n = 18 for cDC2, n = 95 for LCs and n = 67 for pDCs). Bubble enrichment patterns (black boxes) highlighted by the selection of gene sets (from Hallmark collection (H) or homemade gene sets) and pairwise comparisons of interest. **(F)** Heatmaps illustrating genes extracted from the overlap of the GSEA leading edges identified by each pairwise comparison between breast tumors enriched only in cDC1 and those enriched only in one of the 3 other DC subsets. Gene expression values were averaged across tumors enriched in only one DC subset and then log2-transformed.

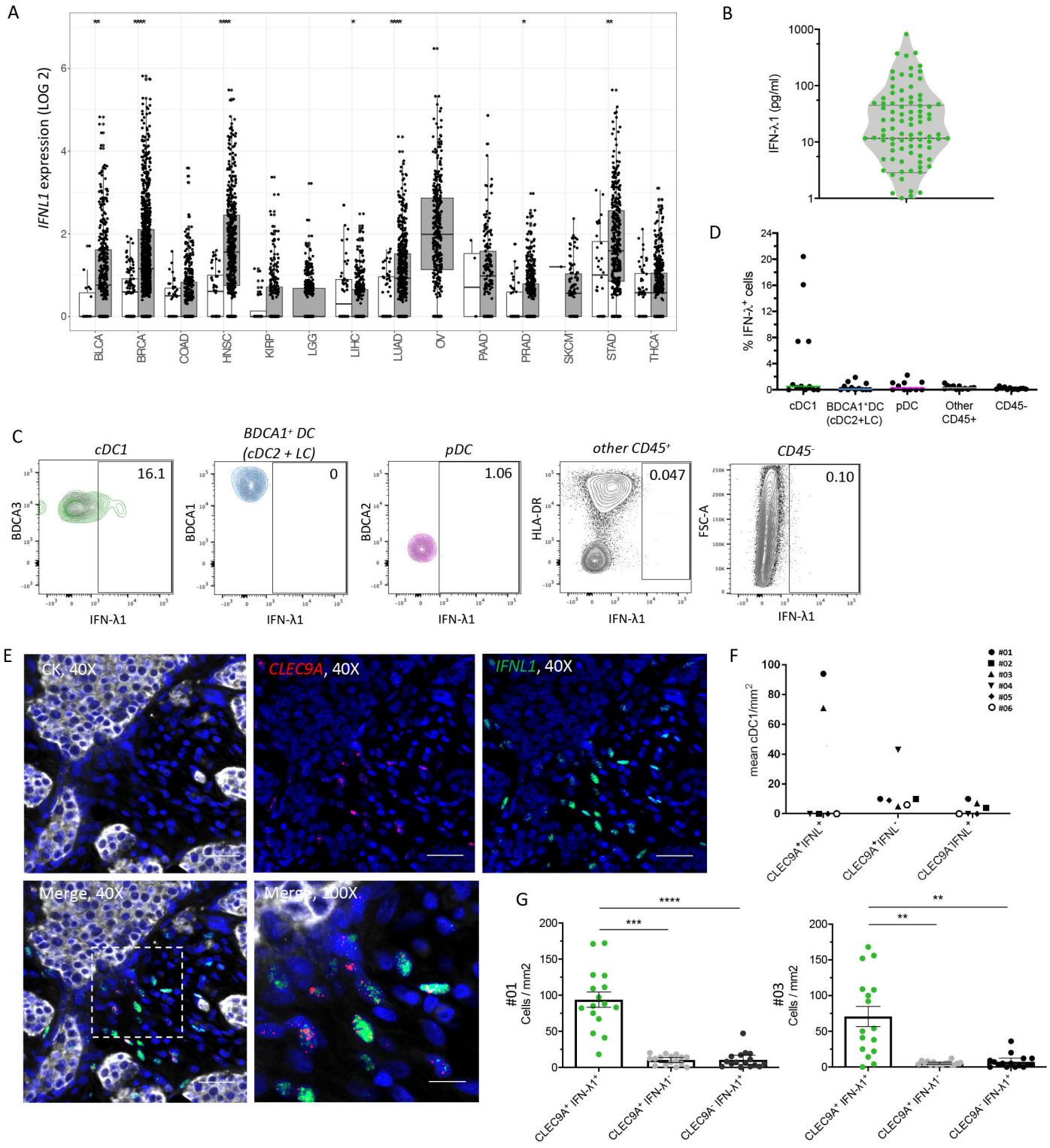

Fig. 5 IFN-λ1 is specifically produced by cDC1 in breast tumors. (A) Differential expression analysis of the *IFNL1* gene in multiple transcriptomic TCGA data sets between the tumor (gray boxes) and the normal adjacent tissue (white boxes). Statistical analysis: Wilcoxon test. **(B)** IFN-λ1 quantification by ECLIA multiplex assay in n = 107 STMs of human breast tumors. **(C)** Intracellular IFN-λ1 FACS staining of one representative breast tumor suspension positive for IFN-λ1 (grey contour plot = isotype control). **(D)** Proportion of IFN-λ1 producing cells in n = 12 breast tumor suspensions. Horizontal bars represent the median of each group of samples. **(E)** *In situ* detection of IFN-λ1 producing cells: *CLEC9A* (red) and *IFNL1* (green) mRNA were stained by duplex RNAscope, combined to an opal-based immunofluorescent staining of cytokeratin-positive tumor cells (white). Nuclei were counterstained with DAPI. White scale bars represent 50 µm for 40X images and 25 µm for 100X images. **(F-G)** Quantification of *IFNL1* and *CLEC9A* simple and double positive cells in 16 randomly-selected zones of 0.64 mm2 per tumor using the Halo software in 6 breast tumors. The mean for each tumor is represented in **(F)** and the exact quantification of the 2/6 *IFNL1*+ tumors (#01 and #03) in **(G)**. Bars and error bars respectively represent the mean and the SEM for each group of samples. Statistical analysis: Friedman test. *p<0.05, **p<0.01, ***p<0.001, ***p<0.0001.

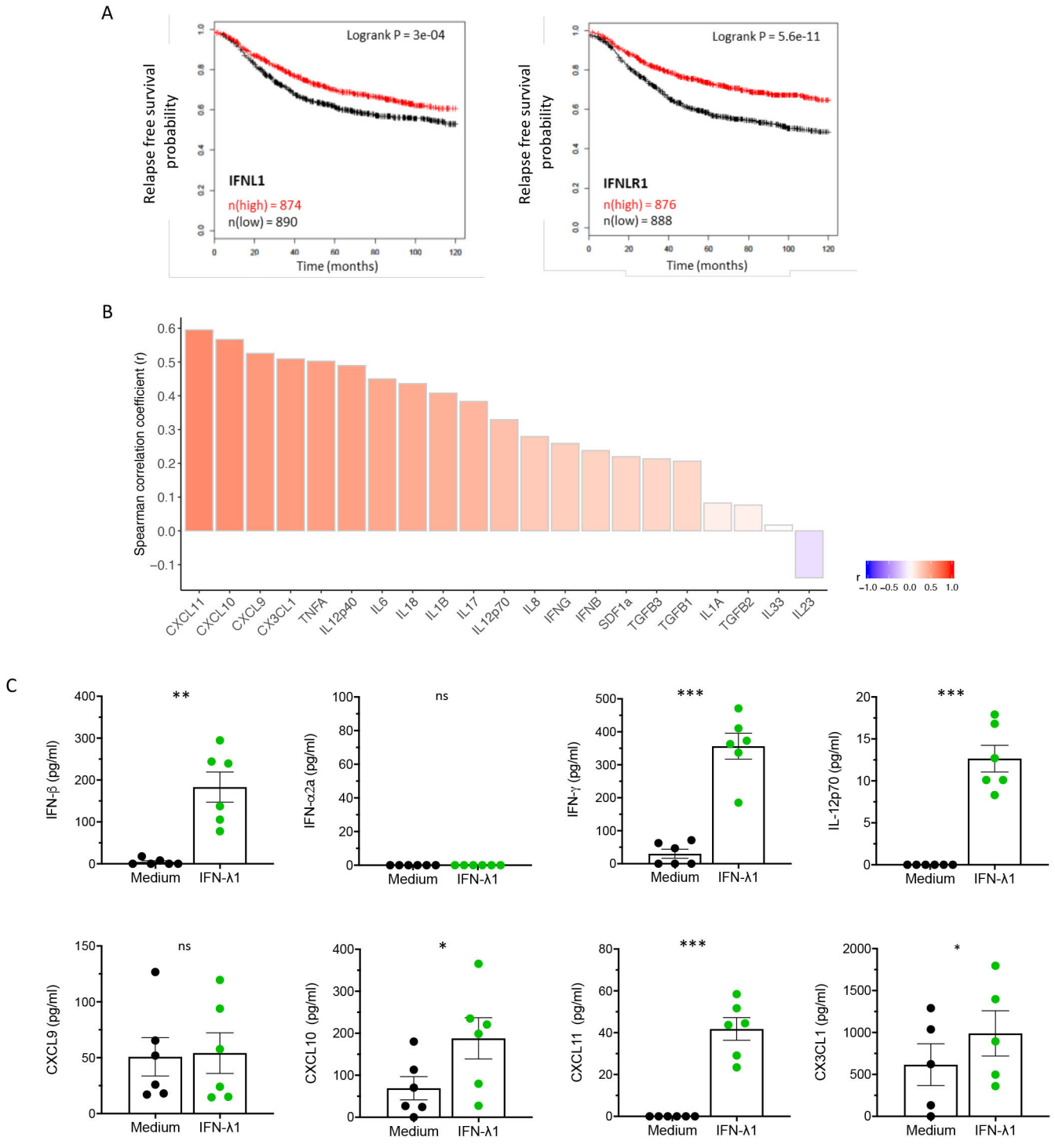

Fig. 6 IFN-λ1 is associated with a favorable outcome and with a Th1 tumor microenvironment in breast cancer. (A) Kaplan-Meier analysis of the relapse-free survival of patients stratified according to the median for the expression of *IFNL1* and *IFNLR1* genes (KMplot transcriptomic data sets). Statistical analysis by log rank test. **(B)** Spearman correlation factors between IFN-λ1 and the other cytokines and chemokines quantified in n = 107 STMs of human breast tumors by ECLIA multiplex assay. **(C)** Cytokine and chemokine quantification by ECLIA multiplex in the supernatants of n = 6 tumor cell suspensions treated or not with IFN-λ1 for 24 h. Bars and error bars respectively represent the mean and the SEM for each group of samples. Statistical analysis: Paired t tests, *p<0.05, **p<0.01, ***p<0.001, ***p<0.0001.

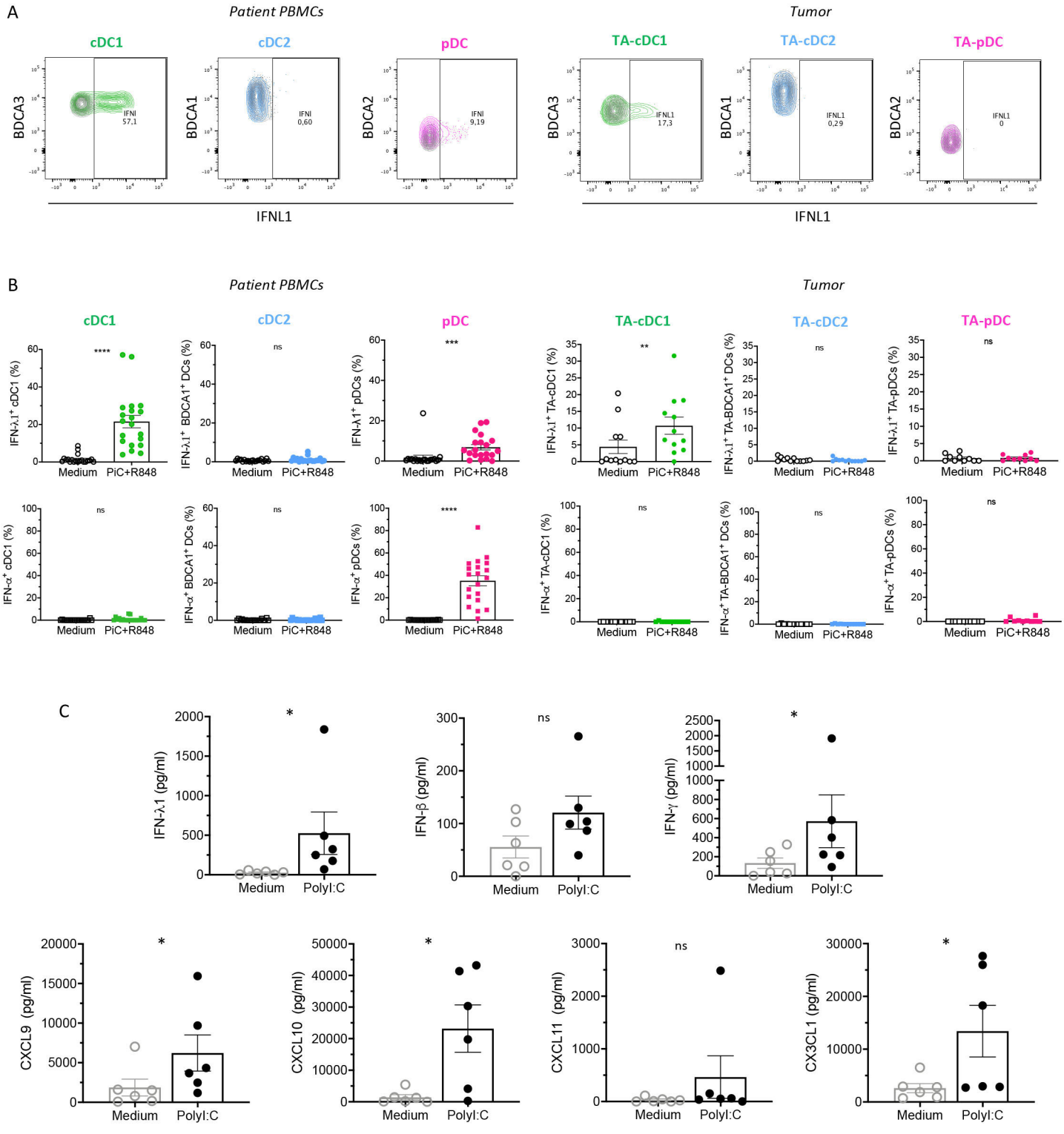

Fig. 7 cDC1 activation by TLR3-L stimulated their IFN-λ1 production and the induction of Th1 immune responses. (A) Representative FACS plots of *ex vivo* IFN-λ1 production by DC subsets from patient PBMCs and breast tumor suspensions treated or not with TLR-L (PolyI:C + R848) for 5h. DC subsets were identified using the gating strategy defined in Fig. 1 and fig S1. **(B)** Proportion of IFN-λ1 and IFN-α producing DC subsets of n = 20 patient PBMCs and n = 12 fresh breast tumor suspensions treated or not with TLR-L (PolyI:C + R848) for 5 h. The medium condition corresponds to Fig. 5C. Bars and error bars respectively represent the mean and the SEM for each group of samples. Statistical analysis: Paired t test. **(C)** Multiplex quantification by ECLIA assay of cytokines and chemokines in the supernatants of n = 6 fresh tumor thick sections treated or not with TLR3-L (Poly(I:C)) for 48 h. Bars and error bars respectively represent the mean and the SEM for each group of samples. Statistical analysis: Wilcoxon test, *p<0.05, **p<0.01, ***p<0.001, ***p<0.0001.

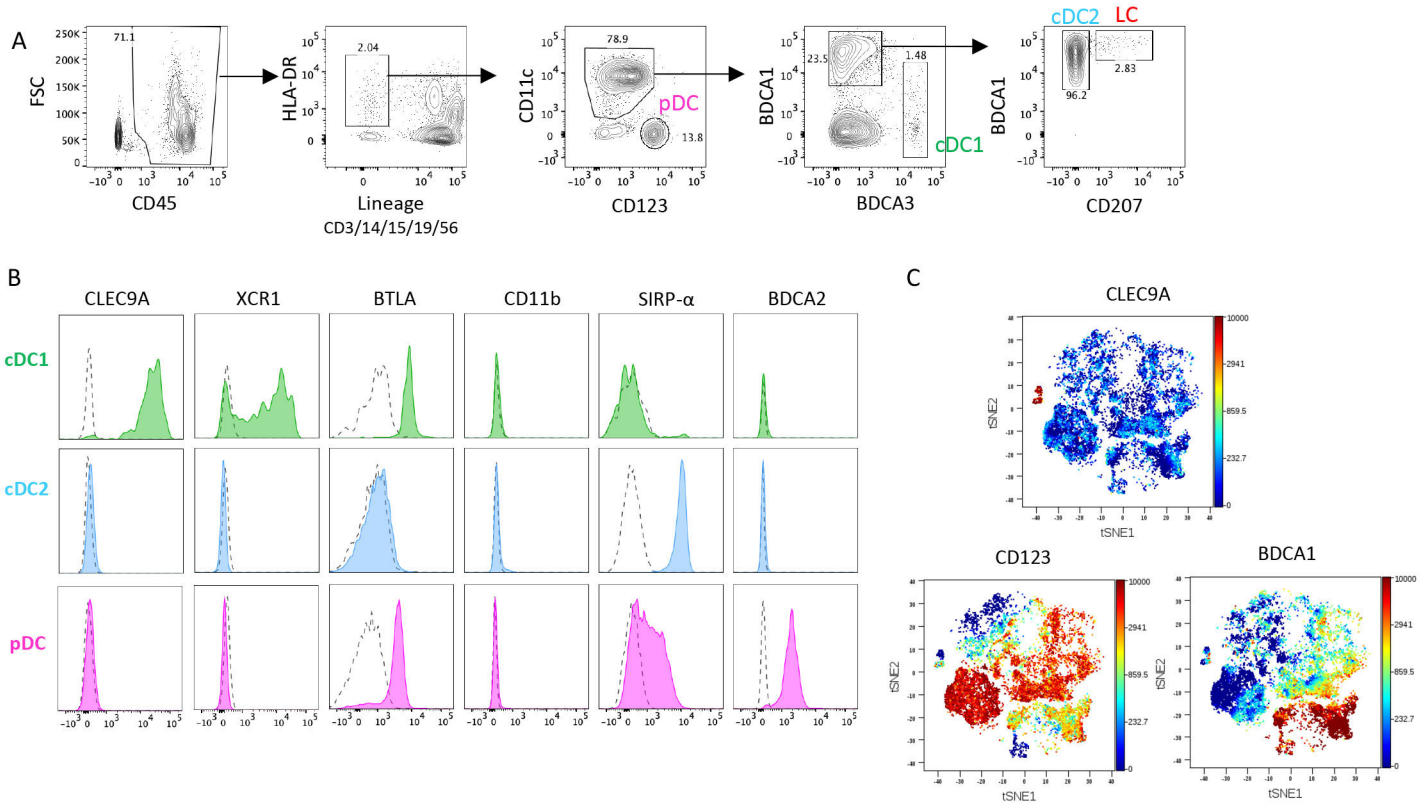

Fig. S1. Identification of DC subsets in patient PBMCs. (A) FACS gating strategy allowing the identification of four DC subsets among viable CD45^{+} HLA-DR^{+} Lineage^{-} (CD3/14/15/19/56) populations in patient PBMCs: pDCs (CD11c^{-} CD123^{+}), cDC1 (CD11c^{+} BDCA1^{-} BDCA3^{hi}), cDC2 (CD11c^{+} BDCA1^{+} BDCA3$^{-/low}$ CD207^{-}) and LCs (CD11c^{+} BDCA1^{+} BDCA3$^{-/low}$ CD207^{hi}). Representative results of n = 10 patients. **(B)** Phenotypic characterization of TA-DC subsets for indicated markers by FACS. Color histogram = indicated marker, dotted line = isotype control. Representative results of n = 8 independent experiments. **(C)** viSNE analysis of viable CD45^{+} HLA-DR^{+} Lin^{-} for the expression of CD11c, CD123, BDCA1, BDCA3, CD207, CLEC9A, CD11b, SIRP-α and BTLA markers, color-coded for the relative expression of FACS markers, with populations indicated (top). Representative results of n = 4 independent experiments.

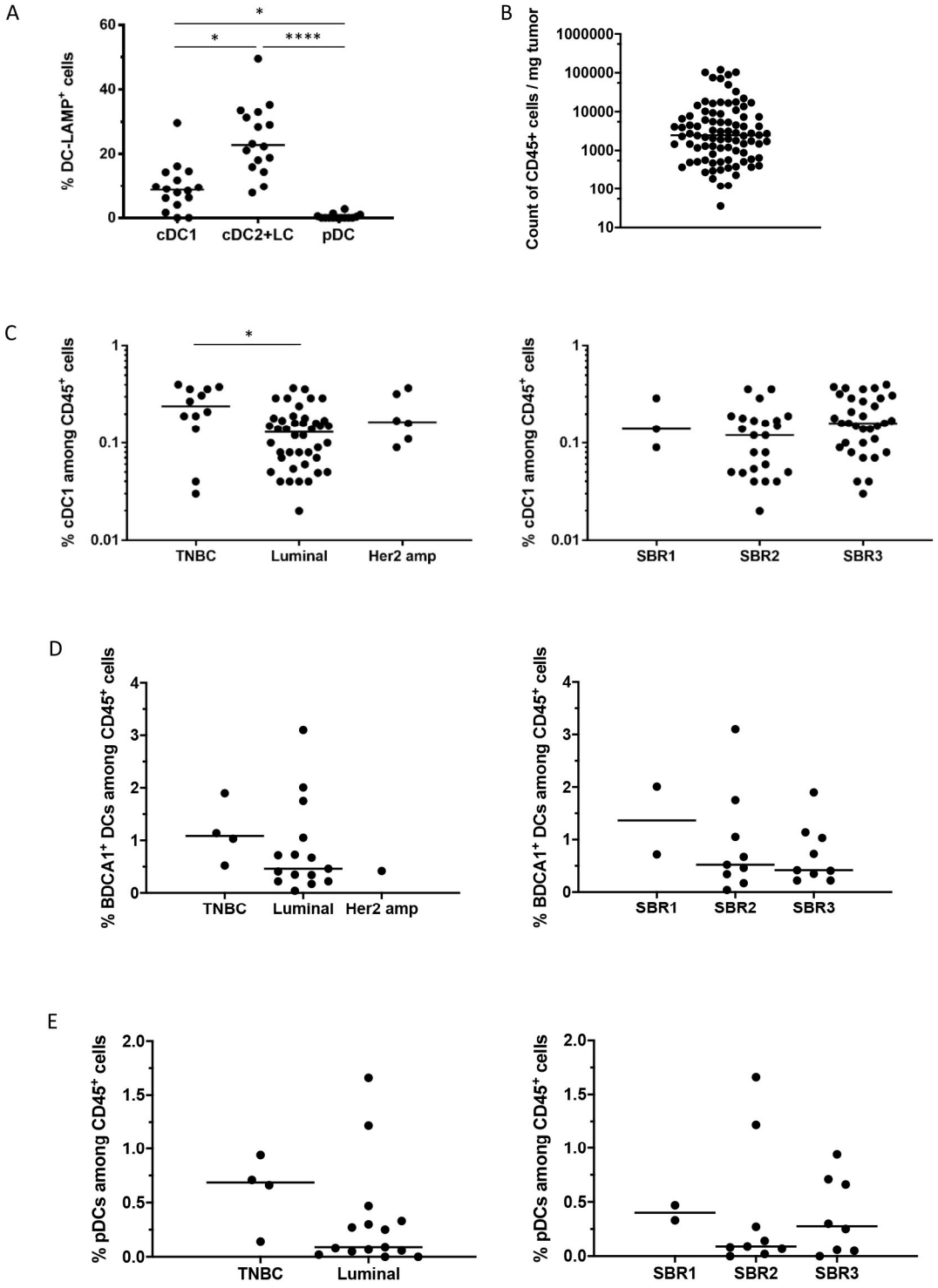

Fig. S2. Proportion of DCs among the immune infiltrate of breast tumors, (A) Proportion of DC-LAMP$^+$ cells among all TA-DC subsets analyzed by FACS. Statistical analysis: Kruskal-Wallis test. **(B)** Number of CD45$^+$ infiltrating cells per milligram of n = 90 breast tumors. **(C-E)** Proportion of cDC1 **(C)**, BDCA1$^+$ DCs **(D)** and pDCs **(E)** (identified with the gating strategy defined in figure S1) among viable CD45$^+$ cells. This was done on different tumor types (TNBC, luminal and Her2 amplified) and grades (SBR1, 2 ,3) in n = 61 breast tumors for cDC1 and in n = 19 breast tumors for BDCA1$^+$ DCs and pDCs. Statistical analysis: Kruskal-Wallis test, Horizontal bars represent the median of each group of samples. *p<0.05, **p<0.01, ***p<0.001, ***p<0.0001.

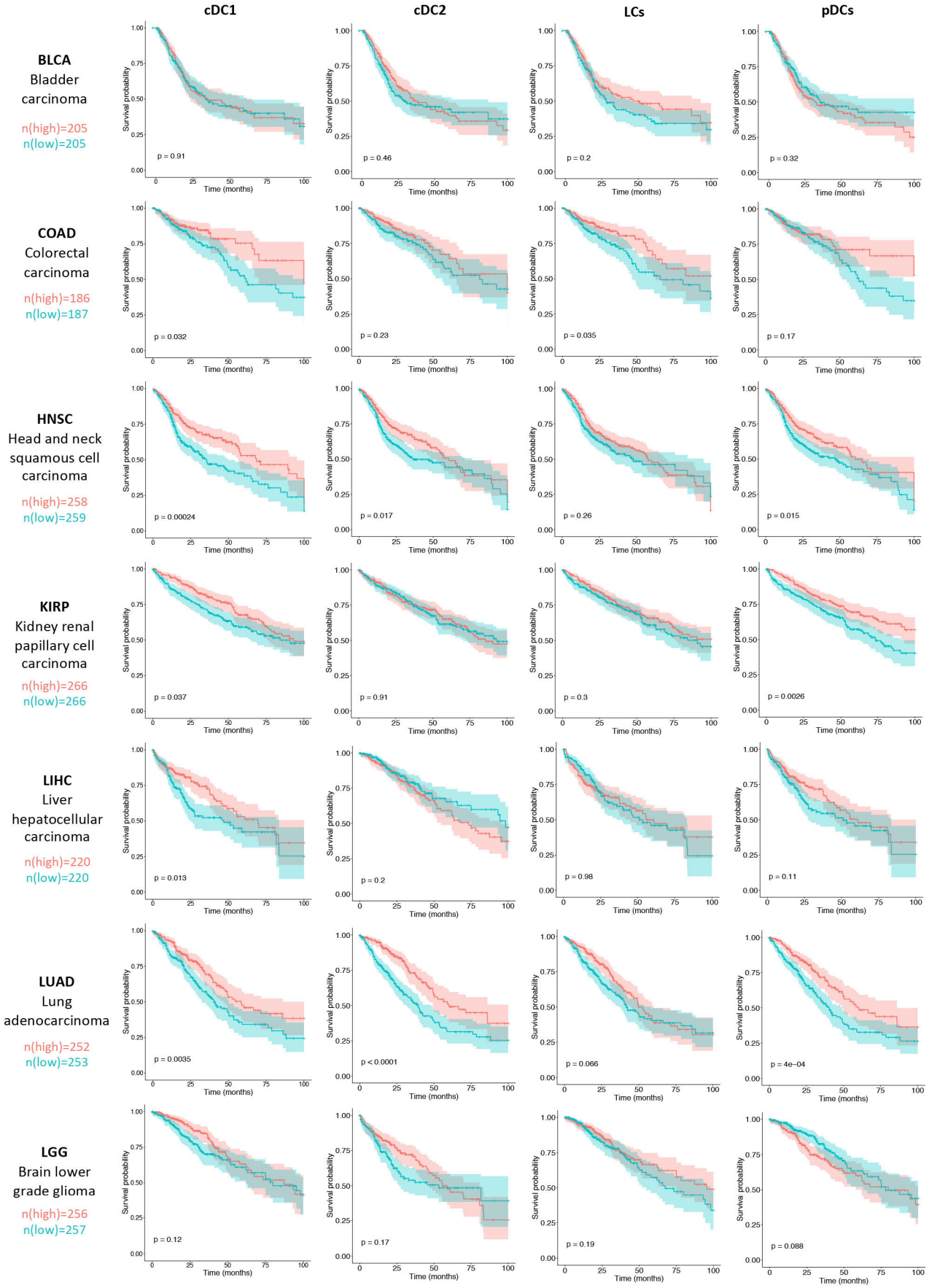

Fig. S3. Kaplan-Meier analysis of the overall survival of cancer patients (Part 1). Patients were stratified according to the median expression score of each DC subset infiltrating in 13 human tumors (calculated with MCP-counter algorithm) using TCGA data sets. Statistical analysis: log rank test.

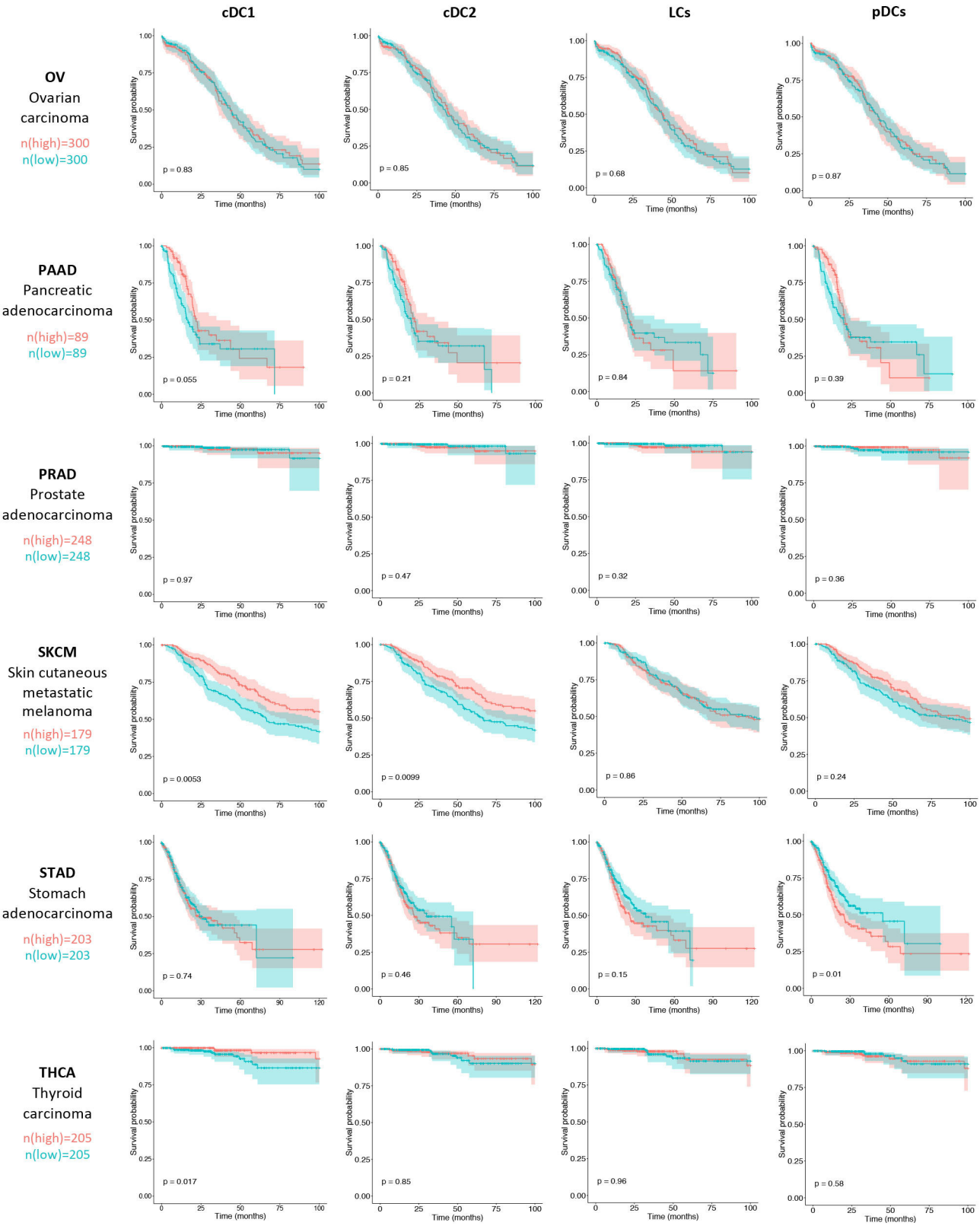

Fig. S3. Kaplan-Meier analysis of the overall survival of cancer patients (Part 2). Patients were stratified according to the median expression score of each DC subset infiltrating in 13 human tumors (calculated with MCP-counter algorithm) using TCGA data sets. Statistical analysis: log rank test.

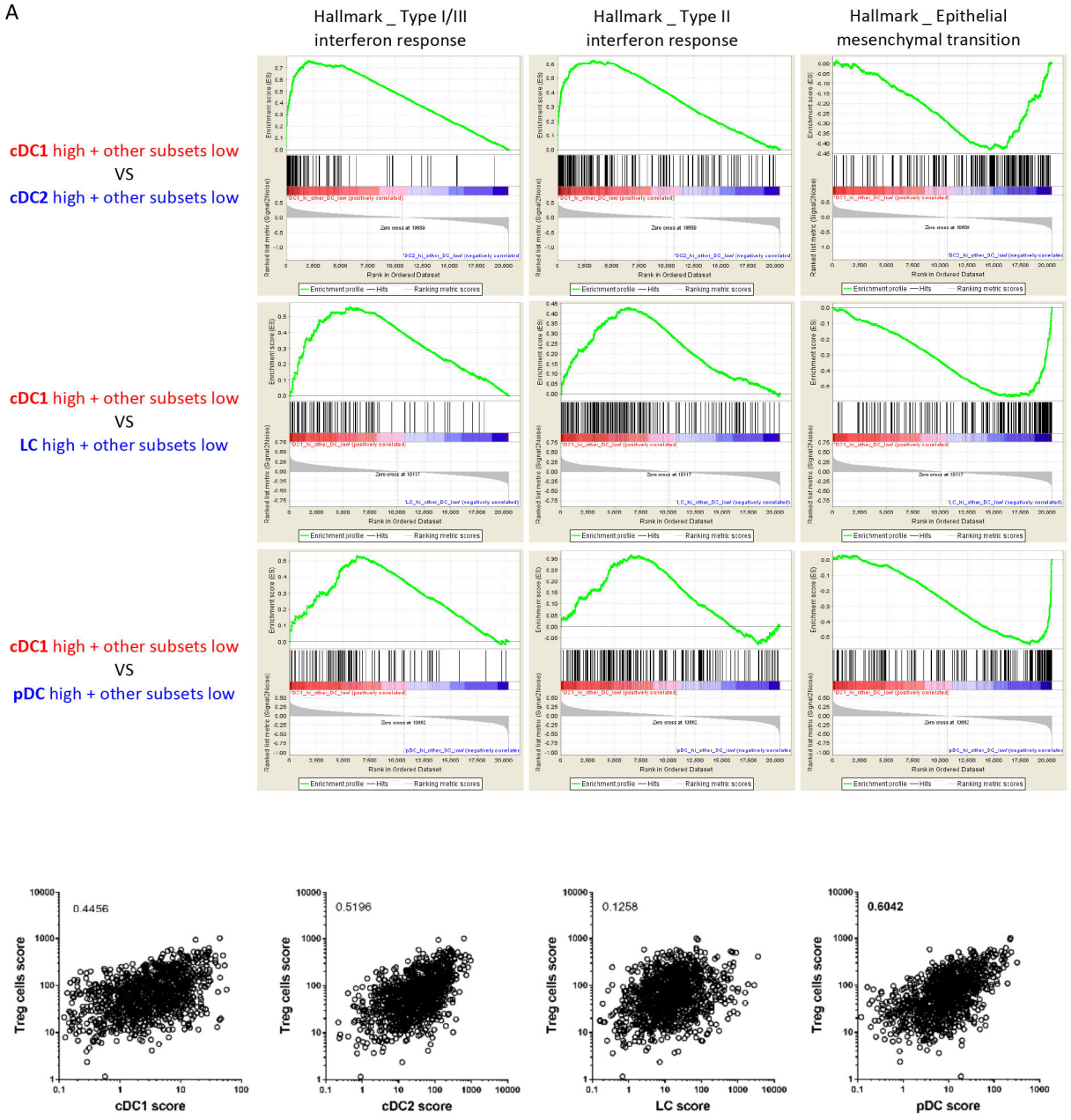

Fig. S4. ***In silico*** **analysis of pathways associated to each DC infiltration score. (A)** Enrichment plots of gene set enrichment analysis between "cDC1-enriched" breast tumors compared with "another DC subset-enriched" breast tumors. **(B)** Scatterplots showing the Spearman correlation between Tregs and each TA-DC subset scores (calculated with MCP-counter algorithm) in n = 1100 breast tumors (TCGA data sets).

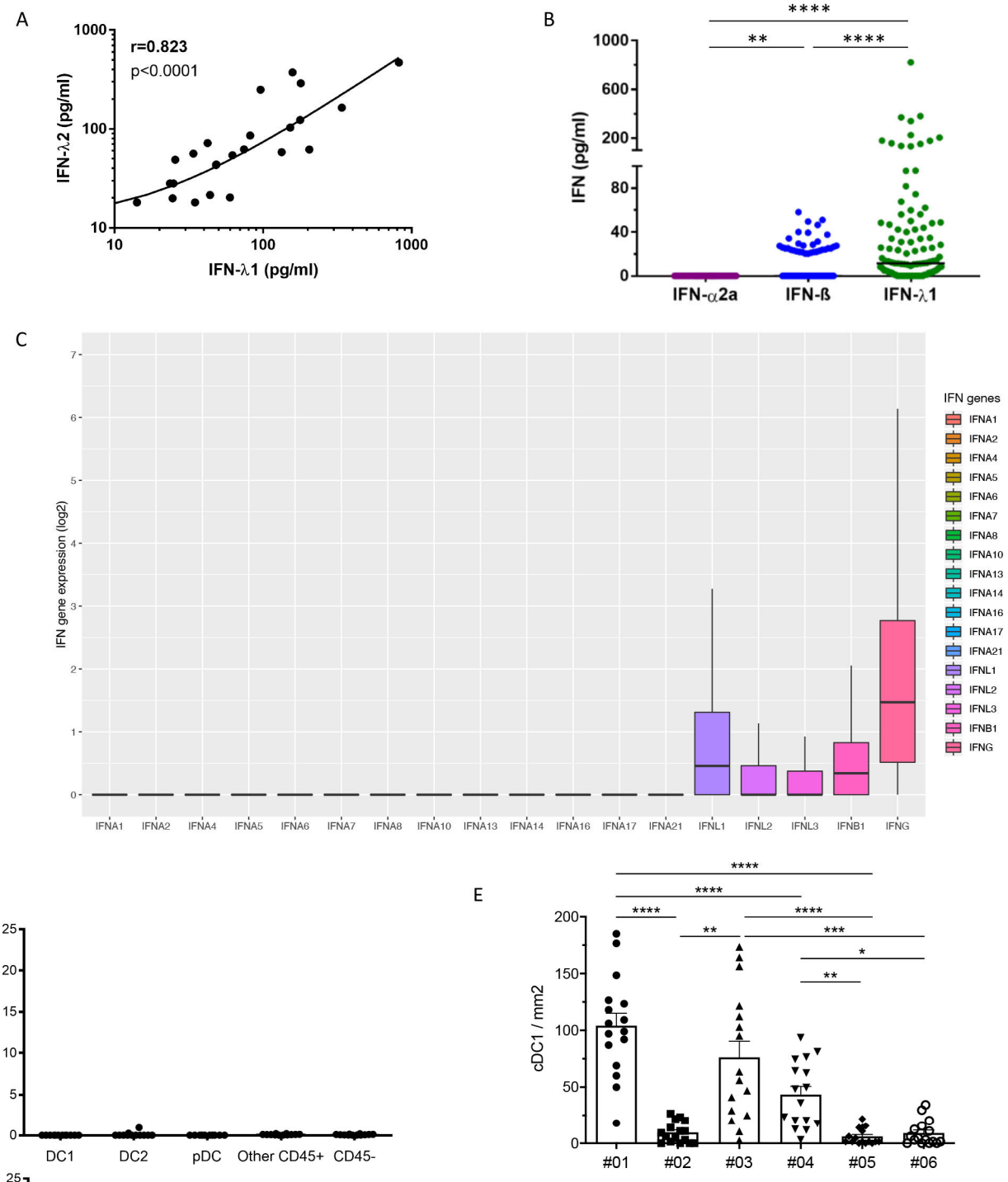

Fig. S5. Quantification of IFNs in breast tumors. (A) Spearman correlation between IFN-λ1 and IFN-λ2 quantified in breast tumor supernatants by ECLIA multiplex assay. **(B)** IFN quantification by ECLIA multiplex assay in n = 107 STMs of human breast tumors. Statistical analysis by Friedman test. **(C)** IFN gene expression in the TCGA data set of breast cancer (n = 1090 patients). **(D)** *Ex vivo* intracellular IFN-α and TNF-α FACS staining in n = 12 fresh breast tumor suspensions without any stimulation. **(E)** Quantification of *CLEC9A* positive cells in n = 6 breast tumors using the Halo software. Bars and error bars respectively represent the mean and the SEM for each group of samples. Statistical analysis: Kruskal-Wallis test. *p<0.05, **p<0.01, ***p<0.001, ***p<0.0001.

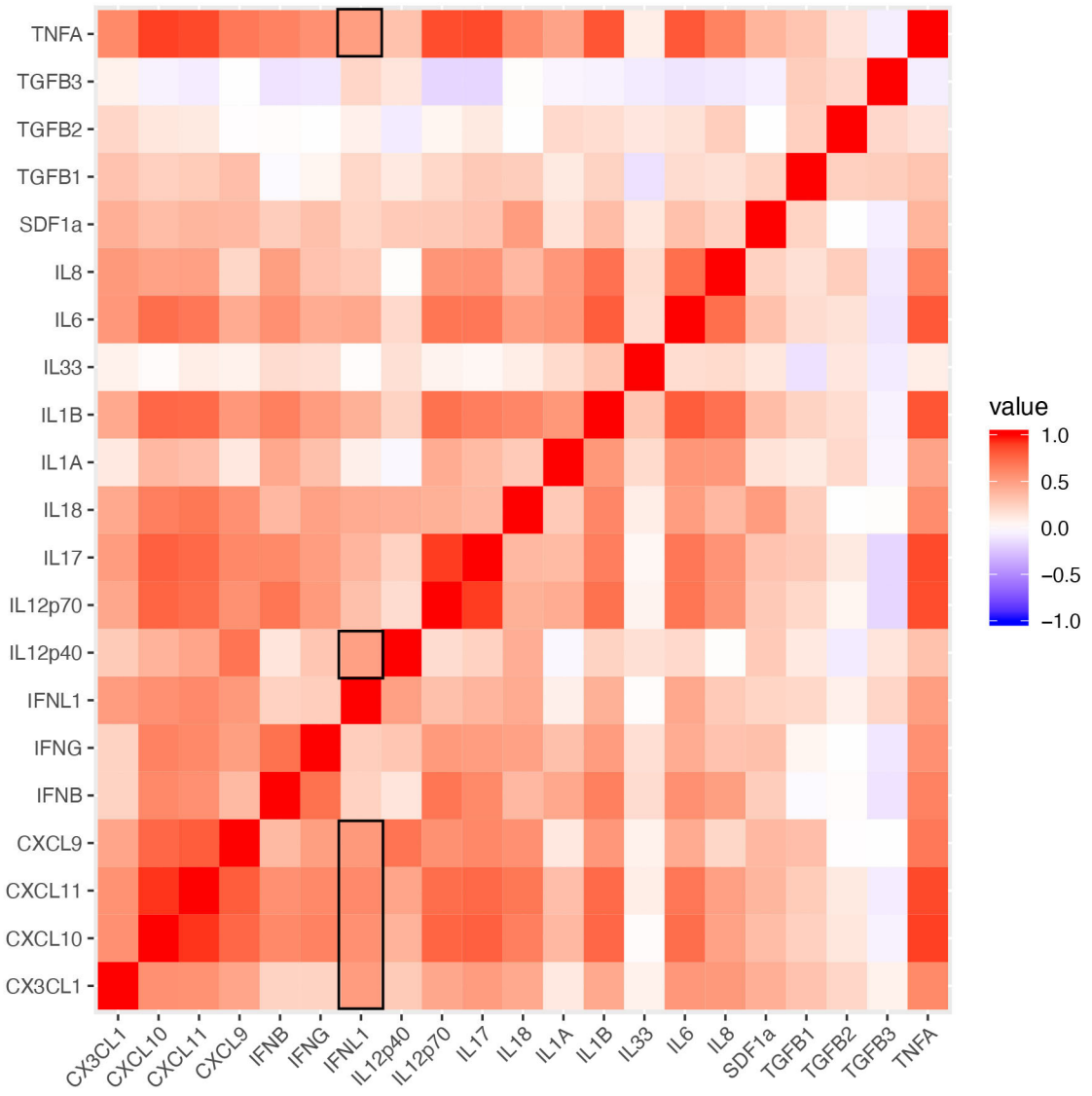

Fig. S6. Correlations between the soluble factors present in human tumors. Heatmap of Spearman correlation coefficients between each cytokine and chemokine quantified in n = 107 STMs of human breast tumor by ECLIA.

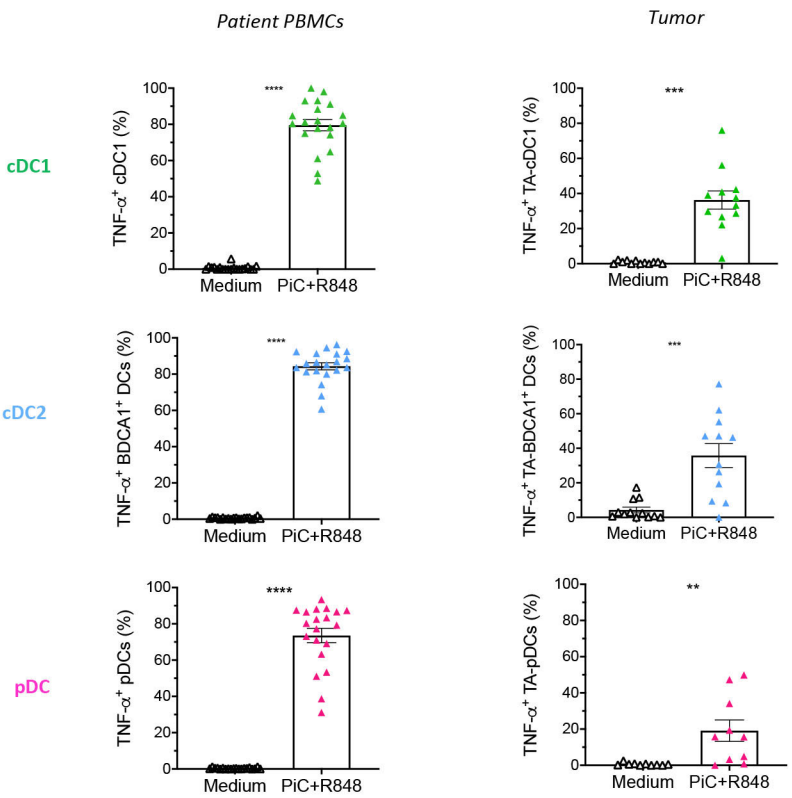

Fig. S7. Analysis of the TNF-α production by DC subsets infiltrating breast tumors. Intracellular TNF-α FACS staining in n = 20 patient PBMCs and n = 12 fresh breast tumor suspensions treated or not with TLR-L (PolyI:C + R848) for 5 h. DC subsets were identified using the gating strategy defined in Fig. 1 and fig S1. Statistical analysis: Wilcoxon test, *p<0.05, **p<0.01, ***p<0.001, ***p<0.0001.

Table S1. FACS antibodies

Marker	Clone	Commercial supplier
CD45	J.33	Beckman Coulter
HLA-DR	L243	Biolegend
CD3	UCHT1	BD
CD14	MϕP9	BD
CD15	HI98	BD
CD19	HIB19	BD
CD56	NCAM16.2	BD
CD11c	Bu15	Biolegend
CD123	7G3	BD
BDCA1	L161	Biolegend
BDCA3	AD5-14H12	Miltenyi
CD207	MB22-9F5	Miltenyi
Clec9A	8F9	Miltenyi
XCR1	S15046E	Biolegend
BTLA	J168-540	BD
CD11b	M1/70.15.11.5	Miltenyi
SIRPa	SE5A5	Biolegend
BDCA2	AC144	Miltenyi
DC-LAMP	104.G4	Beckman Coulter
IFN-λ	MAB15981	R&D
IFN-α	7N4-1	BD
TNF-α	MAb11	BD

Table S2. Immunosuppression gene signature

ARG1	SIGLEC7
CD200	SIGLEC9
CD200R1	TIGIT
CD33	TNFRSF14
CD47	KIR2DL1
CEACAM1	KIR2DL3
COX2	KIR2DL4
CSF1R	KIR3DL1
ENTPD1	KIR3DL2
HLA-E	KIR3DL3
HLA-G	TGFB1
HMOX1	TGFB1I1
IDO1	TGFB2
IDO2	TGFB3
IL10	TGFBI
IL27	VEGFA
IL4I1	VEGFB
KLRC1	VEGFC
KLRD1	ADA
LAIR1	CAMP
LILRB1	PRKACA
LRRC32	SLC29A1
NT5E	ENPP1
PVR	ADK